MAGNETIC CHARACTERISTICS OF CARBONIFEROUS CONTINENTAL DEPOSITIONAL SYSTEMS: IMPLICATIONS FOR THE RECOGNITION OF DEPOSITIONAL HIATUSES

Frank B. Evans

Thesis submitted to the Graduate Faculty of

Virginia Polytechnic Institute and State University

in partial fulfillment of the requirements of the degree of

MASTER OF SCIENCE

in

GEOSCIENCES

Kenneth A. Eriksson, Chair

Richard D. Law

Michal Kowalewski

April 13, 2006

Blacksburg, Virginia

Keywords: Carboniferous, Paleosols, Sandstone, Diagenesis, Rock magnetism, Magnetic hysteresis, Appalachian Basin

MAGNETIC CHARACTERISTICS OF CARBONIFEROUS CONTINENTAL DEPOSITIONAL SYSTEMS: IMPLICATIONS FOR THE RECOGNITION OF DEPOSITIONAL HIATUSES

by

Frank B. Evans

Abstract

Quaternary magnetic studies have provided the conceptual framework to bridge magnetic studies into ancient systems. In cases where environmental materials have been subjected to diagenetic alteration two questions come to mind: 1) What part of the magnetic signal is preserved in the rocks; and 2) can the preserved signal be used to infer/identify magnetic patterns that are characteristic of the depositional, post-depositional, and/or diagenetic environment. Analyses of multi-parameter magnetic experiments conducted on upper Mississippian and lower Pennsylvanian continental successions reveal that distinct depositional, pedogenic, and diagenetic magnetic patterns can be separated and identified. Evidence for a primary depositional signal in several of the upper Mississippian lithofacies is identified by a detrital remanence component attributed to source-area-derived magnetite/titanomagnetite. Red and gray vertisols preserve a Mississippian pedogenic signal characterized by magnetic enrichment, depletion, and amalgamation patterns that are associated with the removal and transport of Fe-rich clays as well as vertical mixing by shrink-swell mechanisms. These well-developed vertisols are interpreted to reflect significant hiatuses in sedimentation associated with prolonged exposure on interfluve/floodplain surfaces that may be correlative with incised valleys (lowstand surface of erosion). Similarly, in lower Pennsylvanian quartz arenite facies, early siderite cementation zones as well as conglomerate lags with distinctive magnetic characteristics are thought to reflect periods of prolonged exposure and to define unconformities within compound valley fills.

Acknowledgements

Completing a M.S. in Geology is truly a marathon event, and I would not have been able to complete this journey without the aid and support of countless people over the past three years. My foremost thank goes to my thesis adviser Dr. Kenneth A. Eriksson. His leadership, support, attention to detail, hard work, and scholarship have set an example I hope to match some day. Without him, this dissertation would not have been possible. I thank him for his patience and encouragement that carried me on through difficult times, and for his insights and suggestions that helped to shape my research skills. His valuable feedback contributed greatly to this dissertation.

I thank the rest of my thesis committee members: Dr. Richard D. Law and Dr. Michal Kowalewski. Their valuable feedback helped me to improve the dissertation in many ways. I am also grateful to my former undergraduate adviser Dr. Whitney J. Autin, who greatly influenced my research tract and encouraged me to pursue a graduate degree in Geology. His visionary thoughts and energetic working style have influenced me greatly as a geologist. Furthermore, he made necessary laboratory and field equipment available to me, and for that I am very grateful. I would also like thank Dr. Kenneth L. Verosub and Dr. Gary Acton, who advised me and helped me with various aspects of my research but notably the acquisition and interpretation of magnetic data collected at the UC Davis Paleomagnetism Laboratory.

I thank all the students and staff in the Virginia Tech Geosciences department, whose presences and fun-loving spirits made the grueling times tolerable. I enjoyed all the vivid discussions we had on various topics and had lots of fun being a member of this fantastic group. I wish to thank Robert J. Bodek in particular: as my friend and collegue, his insights and comments were invaluable over the years, and I look forward to a continuing collaboration with him in the future. Last but not least, I thank my parents Cecilia and Mark, for always being there when I needed them most, and for supporting me through all these years. Partial funding for my research was provided by a grant from the Geological Society of America.

Contents

Abstract..... ii
Acknowledgements..... iii
Introduction..... 1
Appalachian Basin: Geologic Setting..... 2
Analytical Methods..... 6
Upper Mississippian Continental Facies..... 10
Geological Background..... 10
Lithofacies A: Sandstone Facies..... 11
Lithofacies B: Gray Mudstone Facies..... 12
Lithofacies C: Gray Vertisol Facies..... 13
Lithofacies D: Red Vertisol Facies..... 14
Lithofacies E: Limestone Facies..... 15
Lower Pennsylvanian Incised-Valley-Fill Facies..... 16
Geological Background..... 16
Lithofacies F: Quartz Arenite Facies..... 16
Lithofacies G: Heterolithic Facies..... 17
Lithofacies H: Dark Mudstone-Sandstone Facies..... 18
Magnetic Characteristics..... 18
Lithofacies A: Sandstone Facies..... 18
Lithofacies B: Gray Mudstone Facies..... 23
Lithofacies C: Gray Vertisol Facies..... 24
Lithofacies D: Red Vertisol Facies..... 25
Lithofacies E: Limestone Facies..... 26
Lithofacies F: Quartz Arenite Facies..... 27
Lithofacies G: Heterolithic Facies..... 32
Lithofacies H: Dark Mudstone-Sandstone Facies..... 32
Correlation of χ_h and χ_{ferri} with M_S..... 34
Temperature Dependent Magnetic Results..... 35
Interpretation of Magnetic Facies..... 40
Upper Mississippian Magnetic Signals..... 40
Lower Pennsylvanian Magnetic Signals: Core WVGS-4..... 45
Lower Pennsylvanian Magnetic Signals: Core MM-1..... 47
Discussion..... 48
Upper Mississippian..... 48
Lower Pennsylvanian..... 50
Conclusion..... 51
References..... 54
Appendix Contents..... 61
Appendix A..... 62
Appendix B..... 78
Appendix C..... 100
Appendix D..... 117
Appendix E..... 138
Appendix F..... 157

List of Figures

Figure 1 Regional Appalachian Basin map..... 3
Figure 2 Stratigraphic column of the upper Mississippian Mauch Chunk Group.....4
Figure 3 Generalized lithostratigraphic chart for the lower and middle Pennsylvanian record...5
Figure 4 Regional map of West Virginia and Virginia showing the study area.....7
Figure 5 Lithologies and magnetic susceptibility measuements from upper Mississippian outcrops and lower Pennsylvanian cores..... 8
Figure 6 Hysteresis loop examples.....10
Figure 7 Upper Mississippian Facies Coercivity of remanence (B_{CR}) vs. Low-frequency magnetic susceptibility (χ_{lf}).....19
Figure 8 Upper Mississippian Facies Day Plot.....20
Figure 9 Upper Mississippian Facies Ferrimagnetic susceptibility (χ_{ferri}) vs. High-field susceptibility (χ_h).....21
Figure 10 Paramagnetic M_S vs. Ferri/antiferromagnetic M_S for upper Mississippian samples....22
Figure 11 Lower Pennsylvanian Facies Coercivity of remanence (B_{CR}) vs. Low-frequency magnetic susceptibility (χ_{lf})..... 27
Figure 12 Lower Pennsylvanian Facies Day Plot.....29
Figure 13 Lower Pennsylvanian Facies Ferrimagnetic susceptibility (χ_{ferri}) vs. Paramagnetic susceptibility (χ_h).....30
Figure 14 Paramagnetic M_S vs. Ferri/antiferromagnetic M_S for lower Pennsylvanian samples...31
Figure 15 High-field susceptibility (χ_h) vs. Paramagnetic M_S for upper Mississippian and lower Pennsylvanian Facies.....34
Figure 16 Upper Mississippian Temperature-dependent susceptibility.....36
Figure 17 Lower Pennsylvanian stepwise thermal hysteresis acquisitions.....38
Figure 18 Lower Pennsylvanian Temperature-dependent susceptibility.....39

Introduction

Extension of Quaternary environmental magnetic techniques (e.g. Verosub and Roberts, 1995; Maher, 1998; Geiss and Banerjee, 1997; Florindo et al., 1999) to the ancient rock record (e.g. Channel and McCabe, 1994; Rankey and Farr, 1997; Soreghan et al., 1997, 2002; Ellwood et al., 2000, 2001; Retallack et al., 2003) has demonstrated that these methods are capable of identifying climatologic, pedologic and diagenetic processes in lithified sedimentary rocks. The above researchers have shown that unique relationships exist between the magnetic properties of detrital grains and authigenic/ post-depositional minerals within alluvial sediments. In well-drained sediments and soils, magnetic patterns primarily arise in response to the mineralogy, concentration, and grain size of iron oxide complexes. In contrast, hydromorphic conditions promote iron reduction and mobilization in which cases iron sulfides and/or other reduced iron complexes may dominate. However, in cases where post-depositional and/or diagenetic conditions occur, the primary magnetic properties (mineralogy, concentration, and/or grain size) may change such that a completely different combination of such properties exists within the altered materials.

Over the past 30 years, magnetic investigations of sedimentary sequences have been used largely to correlate climatic changes with pedogenic modification of sedimentary units. Recent studies (e.g. Beget et al, 1990; Verosub et al., 1993; Maher and Thompson, 1995; Geiss, 1997; Maher, 1998; Florindo et al, 1999; Virina et al, 2000; Evans, 2001; Evans and Heller, 2001; Porter, 2001) have demonstrated the usefulness of magnetic properties of sediments as proxy indicators for paleoclimate. Studies on Quaternary sediments of the Chinese Loess Plateau concluded that magnetic susceptibility maxima occur in intercalated paleosols (associated with warm interglacials) and susceptibility minima occur in unaltered loess (associated with dry cool glacial times) (Heller and Liu, 1984; Kukla et al., 1988; Liu et al., 1992). Many authors have attributed this enhancement to the *in situ* production of very fine magnetite and/or maghemite grains under oxidizing conditions (e.g. Liu et al., 1992; Verosub et al., 1993; Evans and Heller, 1994; Heller and Evans, 1995). However, studies in Alaska (Begét et al., 1990) and Siberia (Chlachula et al., 1998) found the opposite relationship; during glacial times, wind-vigor was able to entrain dense magnetic particles into the atmosphere resulting in susceptibility maxima within unaltered loess sections. Studies in Russia and the Ukraine (e.g. Tsatskin et al., 1998) documented magnetic depletions within some reduced paleosol profiles where hydromorphic

conditions caused chemical degradation (and eventual removal) of magnetite leading to a decrease in magnetic susceptibility, which has been termed the "gleying" model.

Whereas a multitude of studies and techniques associated with natural and synthetic magnetic materials exist, the great majority are related to unlithified Quaternary strata. In comparison to present day cases, little work has been conducted on ancient sedimentary systems, and even less on ancient continental fluvial/ alluvial strata, to determine the processes and pathways that a magnetic material follows from the time it is deposited through its burial and exhumation (e.g. Channel and McCabe, 1994; Rankey and Farr, 1997). Quaternary magnetic studies have provided the conceptual framework to advance magnetic studies into ancient systems. In cases where environmental materials have been subjected to diagenetic alteration two questions arise: 1) What part of the magnetic signal is preserved in the rocks; and 2) can the preserved signal be used to infer/identify magnetic patterns that are characteristic of the depositional, post-depositional, and/or diagenetic environments. These fundamental questions need to be addressed in sedimentary rocks where the influence of burial compaction, temperature, and pore fluid chemistry may have modified the magnetic properties present at the time of deposition.

This study is concerned with identifying distinct syndepositional and diagenetic magnetic patterns in Carboniferous fluvial/ alluvial strata in the Central Appalachian Basin (Fig. 1). Unique diagenetic changes preserved in these rocks arise as a product of the initial environmental conditions present at the time of deposition. The hypothesis of the study is that diagenetic overprinting alters the primary magnetic characteristics present at the time of deposition within continental fluvial/ alluvial strata. In unique circumstances, the magnetic character of the diagenetically altered magnetic material can be used to identify primary magnetic patterns, and in certain situations, be used to identify diagenetically-modified, subaerially-exposed facies. By combining field observations in Carboniferous fluvial and alluvial facies with multi-parameter magnetic techniques, the identification and characterization of lithofacies in ancient continental fluvial strata can be magnetically linked to modern analogs.

Appalachian Basin: Geologic Setting

Multiple episodes of Paleozoic tectonic collisions resulted in development of the Appalachian Foreland Basin (Dewey, 1981). In response to subsidence and deposition related to

thrust loading in the hinterland, as much as 7 km of Middle Ordovician to Lower Permian strata were deposited in the Central Appalachian Basin (Quinlan and Beaumont, 1984) that is bounded to the southeast by the Appalachian fold and thrust-belt and to the west by the Cincinnati Arch (Fig. 1).

This study focuses on the upper Mississippian Mauch Chunk Group and the lower Pennsylvanian New River Formation. The Mauch Chunk Group in West Virginia consists of the

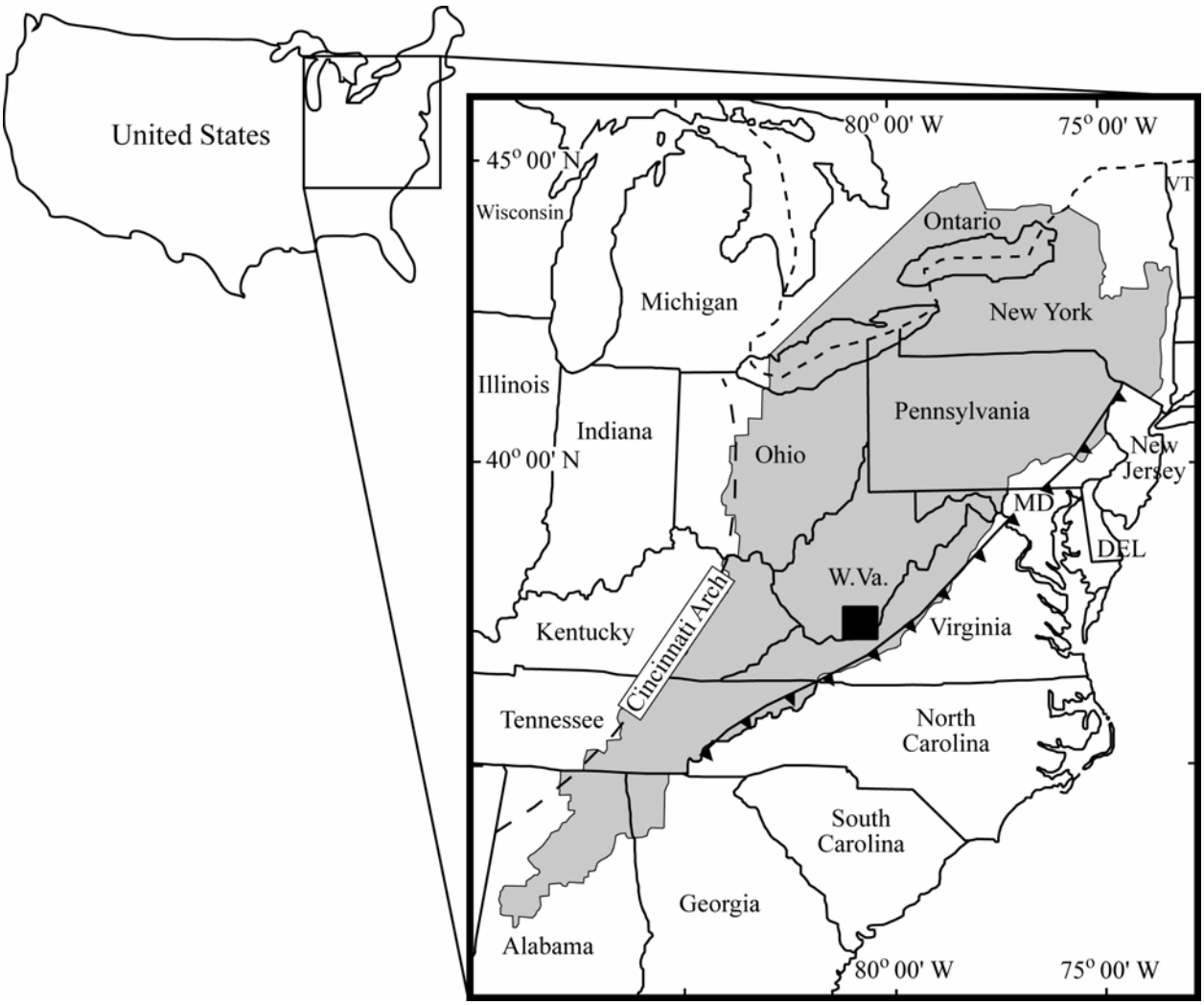

Figure 1 - Location map of the Appalachian Basin (shaded). Study area is shown by the shaded box. Aerial extent of the Appalachian Basin, Swezey (2002). The western Appalachian Basin boundary (the Cincinnati Arch), Greb et al. (2000 and 2004). The eastern Appalachian Basin boundary (the fold-thrust front), Englund and Thomas (1989).

Hinton, Princeton, and Bluestone formations (Fig. 2) that comprise an east-southeastward-thickening clastic wedge that reaches a maximum thickness of ~600 meters in Mercer County

(Miller and Eriksson, 1999)**.** Biostratigraphic data compiled by Miller (1998) indicate that the base of the study interval correlates with the lower Namurian A (Pendleian), and that the top is no younger than the middle/late Namurian A (middle Arnsbergian). The Carboniferous time scale provided by Davydov et al. (2004) give estimates of 326.4 ? 1.6 Ma for the lower boundary

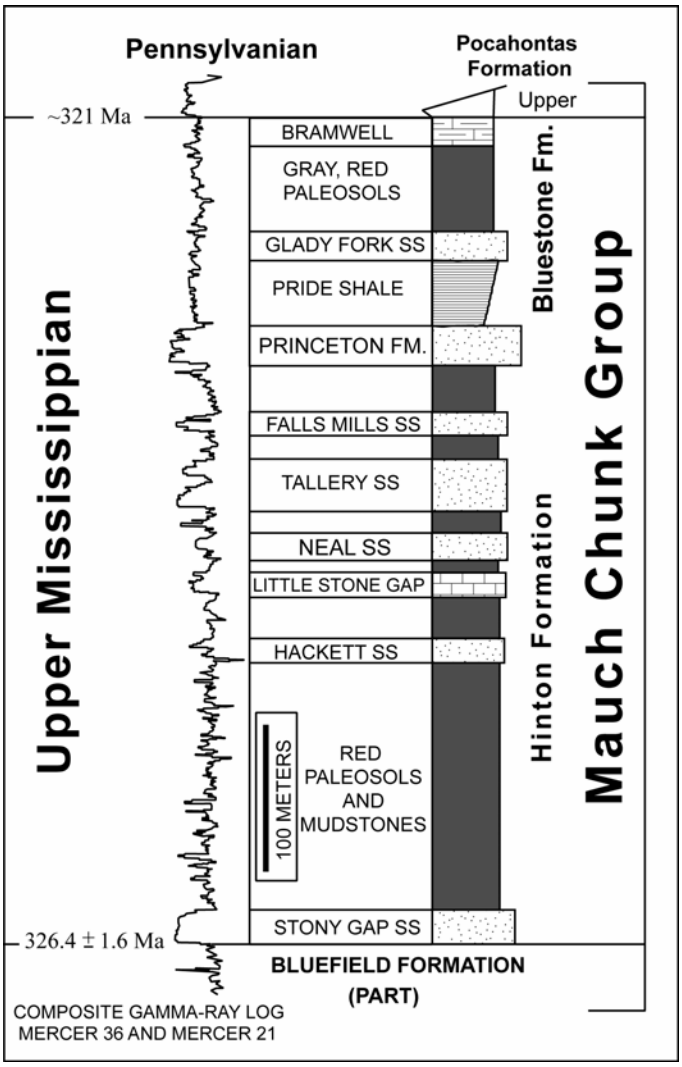

Figure 2 - Stratigraphic column of the upper Mississippian Mauch Chunk Group in the Central Appalachian Basin showing typical gamma-ray signature from west Mercer County W.V. (Miller and Eriksson, 2000). Age constraints are based on biostratigraphic data compiled by Miller (1998) and the Carboniferous Time Scale of Davydov et al. (2004).

and ~ 321 Ma for the upper boundary. Therefore, the duration of the study interval is ~ 5.6 Myr. Subsurface correlation of the Mauch Chunk Group shows that these facies extend over some 15,000 km^2 into adjacent parts of Virginia and Kentucky (Miller and Eriksson, 2000). Tectonic highlands along the southeastern margin of the central Appalachian basin provided the source of sediments for the Mauch Chunk terrigenous units (Englund and Thomas, 1990; Miller and Eriksson, 2000). During the Late Mississippian, the region moved northward into sub-equatorial

latitudes, in which a semiarid to seasonal climate prevailed (Cecil, 1990; Beauthin and Blake, 2002).

The lower Pennsylvanian New River Formation in West Virginia consists of ~300 meters of predominantly nonmarine siliciclastics (Klein and Willard, 1989) that onlap to the northwest and thicken towards the southeast of the basin (Englund and Thomas, 1990). In West Virginia, the New River Formation is dominated by several quartz-rich sandstone bodies that are named (from bottom to top) the Pineville, Lower Raleigh, Upper Raleigh, Guyandot, Lower Nuttall, and Upper Nuttall sandstones (Fig. 3). New River Formation sandstone bodies are part of the distal foreland basin deposits that interfinger towards the thrust front (Fig. 1) with marginal marine and subordinate nonmarine strata (Englund and Tomas, 1990; Korus, 2002). Studies indicate (e.g.

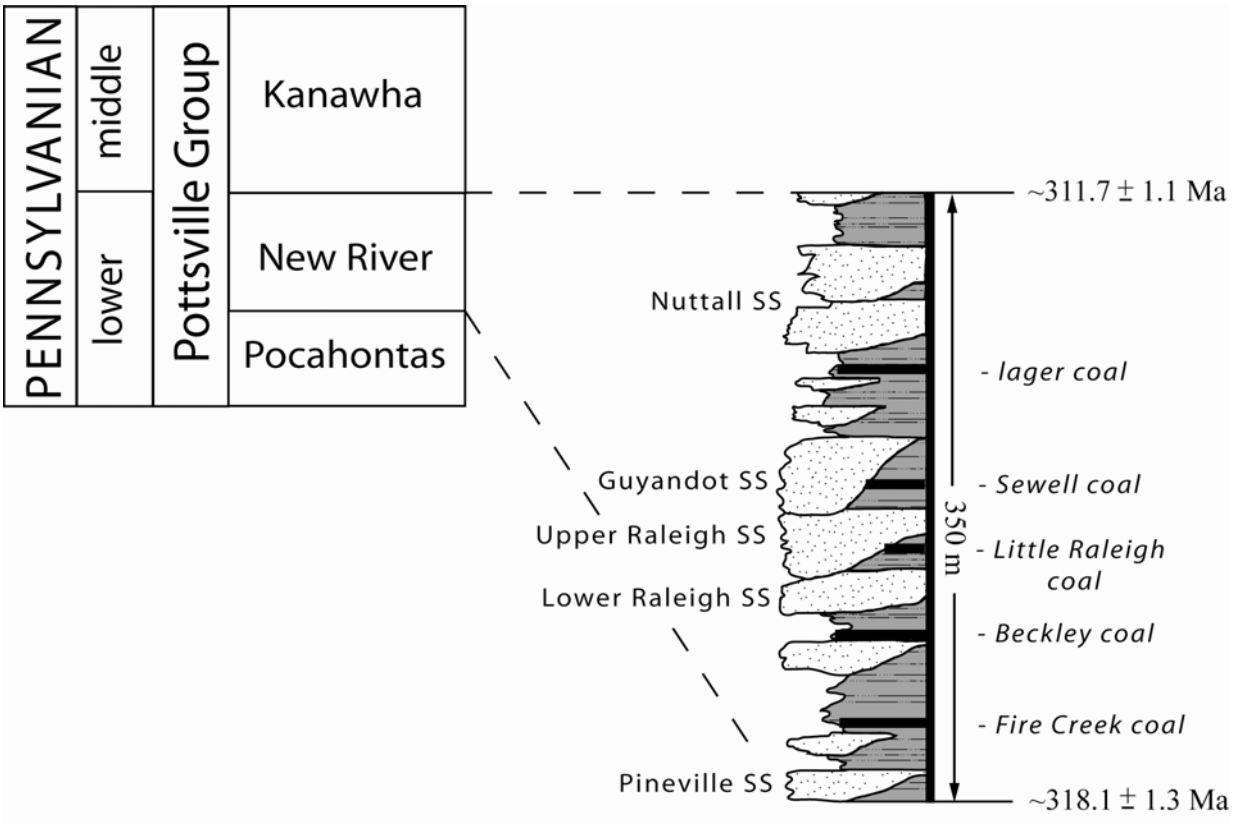

Figure 3 - Generalized lithostratigraphic chart for the lower and middle Pennsylvanian record of the Central Appalachian Basin from Korus (2002). Detailed column shows typical lithologies of the New River Formation. The names of major sandstone bodies and mineable coal seams are given. Age estimates are based on megafloral biostratigraphy by Blake (1997) and correlation with western European stages (Riley and Turner, 1995). The Carboniferous time scales provided by Davydov et al. (2004) give estimates for the lower and upper boundaries of the New River Formation.

Blake, 1997; Riley and Turner, 1995) that the interval between the base of the New River Formation and the base of the Kanawha Formation (Fig. 3) corresponds to the Namurian B/C Westphalian A/B. The Carboniferous times scales provided by Davydov et al. (2004) give estimates of 311.7 ? 1.1 Ma for the upper boundary and 318.1 ? 1.3 Ma for the upper boundary of this stage. Therefore, the duration of the study interval is ~ 6 Myr.

Analytical Methods

Three upper Mississippian outcrops were studied: PWV-1 and PHS-1 are exposed road-cuts along Highway 460 east of Princeton, West Virginia, while SSWV-1 is located along I-64 near Sandstone, West Virginia (Fig. 4). Two Lower Pennsylvanian cores that spanned the Upper and Lower Raleigh sandstones were obtained from coal-bed methane exploration test wells. The first, WVGS-4, is located ~15 miles northeast of Beckely near I-64 and the second, MM-9 is located ~10 miles west of Beckely near Bolt, W.Va. off of Rt. 99 (Fig. 4). The three upper Mississippian outcrops were logged at 10 cm intervals (Fig. 5a to c). In WVGS-4, specific intervals were measured that were previously analyzed for thin-section, microprobe, and fluid inclusion studies by Reed et al. (2005) (Fig. 5d). The second core, MM-9 was logged at 10 cm intervals (Fig. 5e). Using a Bartington MS2 susceptibility meter with surface scanning sensor (MS2K), volume magnetic susceptibility (?) data were collected on outcrop from the Mauch Chunk Formation and from core for the Upper and Lower Raleigh sandstones. In order to obtain representative ? values, care was taken to avoid siderite and quartz clasts within conglomeratic intervals in core WVGS-4.

Upper Mississippian paleosols were analyzed in the field using the methods described by Retallack (1988). By the use of a portable gas-powered drill, 50 upper Mississipian outcrop samples were collected from the three outcrops for magnetic characterization. Representative samples from each lithofacies were collected, as well as samples with anomalous ? values. A total of 56 samples from core WVGS-4 were selected, categorized by lithofacies, and ? measured. Selected samples studied by Reed et al. (2005) from this core were also described and used for magnetic analysis. A total of 908 continuous samples from core MM-9 samples were described, categorized by lithofacies, and ? measured. Based on lithology and ? patterns, representative samples were chosen from the core for detailed magnetic characterization.

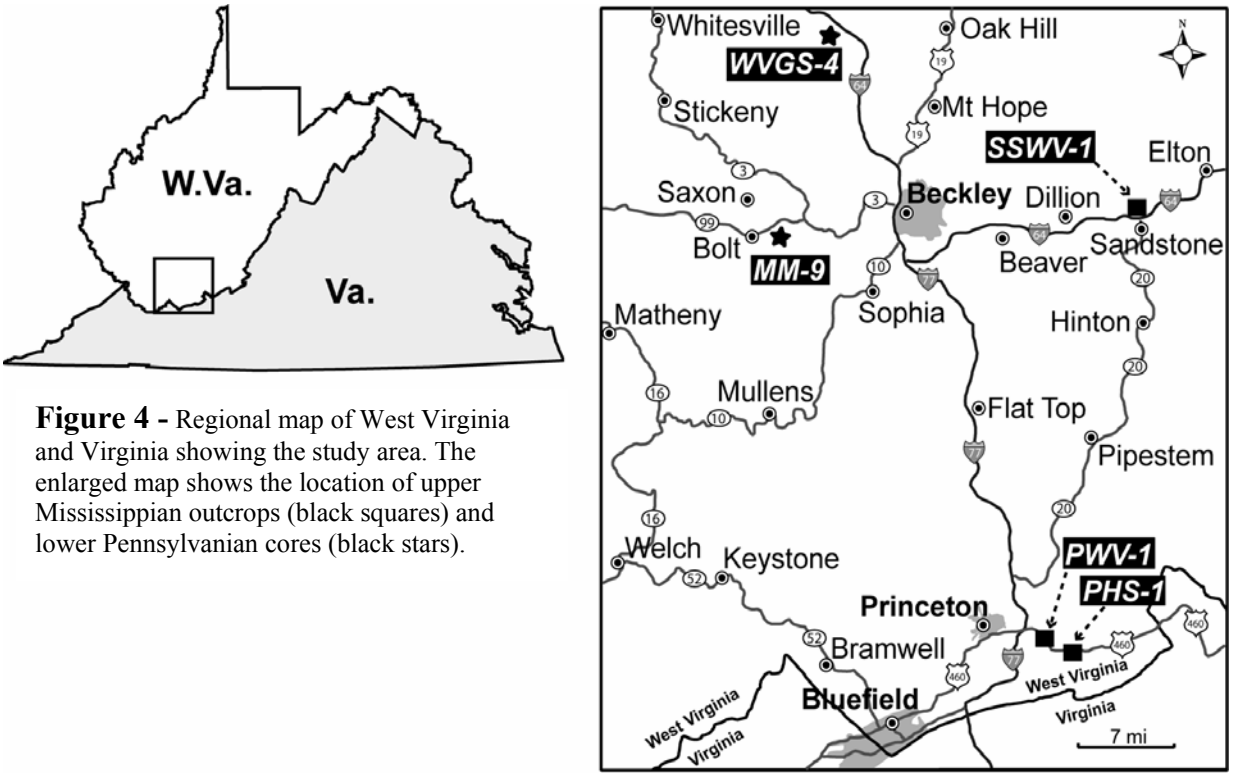

Figure 4 - Regional map of West Virginia and Virginia showing the study area. The enlarged map shows the location of upper Mississippian outcrops (black squares) and lower Pennsylvanian cores (black stars).

For magnetic analysis, all representative outcrop and core samples were measured at the UC Davis Paleomagnetism Laboratory in Davis, CA for: (1) frequency-dependent magnetic susceptibility ($\chi_{fd\%}$) using a Bartington Instruments MS2B Dual Frequency Sensor with an AC magnetic field amplitude of 80 Am^{-1} at low frequency (χ_{lf}, 465 Hz) and high frequency (χ_{hf}, 4650 Hz) ($\chi_{fd\%}$ for all the samples measured was less than 1% and, therefore, superparamagnetic contributions are considered to be negligible for all of the samples measured); and (2) hysteresis properties (M_S, M_{RS}, B_C, B_{CR}, χ_d and χ_h; Fig. 6) using a Princeton Instruments MicroMag 2900 alternating gradient magnetometer. The hysteresis properties obtained for each sample were normalized on a per mass [kg] basis. For selected samples, additional temperature-dependent susceptibility measurements (TDS) were conducted on a Kappabridge KLY-3S with CS-3 furnace apparatus from room-temperature to 700^oC and then back. Sequential step-wise heating experiments were conducted on selected samples by measuring hysteresis properties at room-temperature after each heating step. Prior to the first heating step, the hysteresis properties of the samples were measured. After the initial measurement, the samples were heated sequentially in O_2 using a non-magnetic furnace at temperatures of 300, 400, 500, 550, and 600^oC. The various magnetic parameters used in this study are explained in Appendix A.

Figure 5

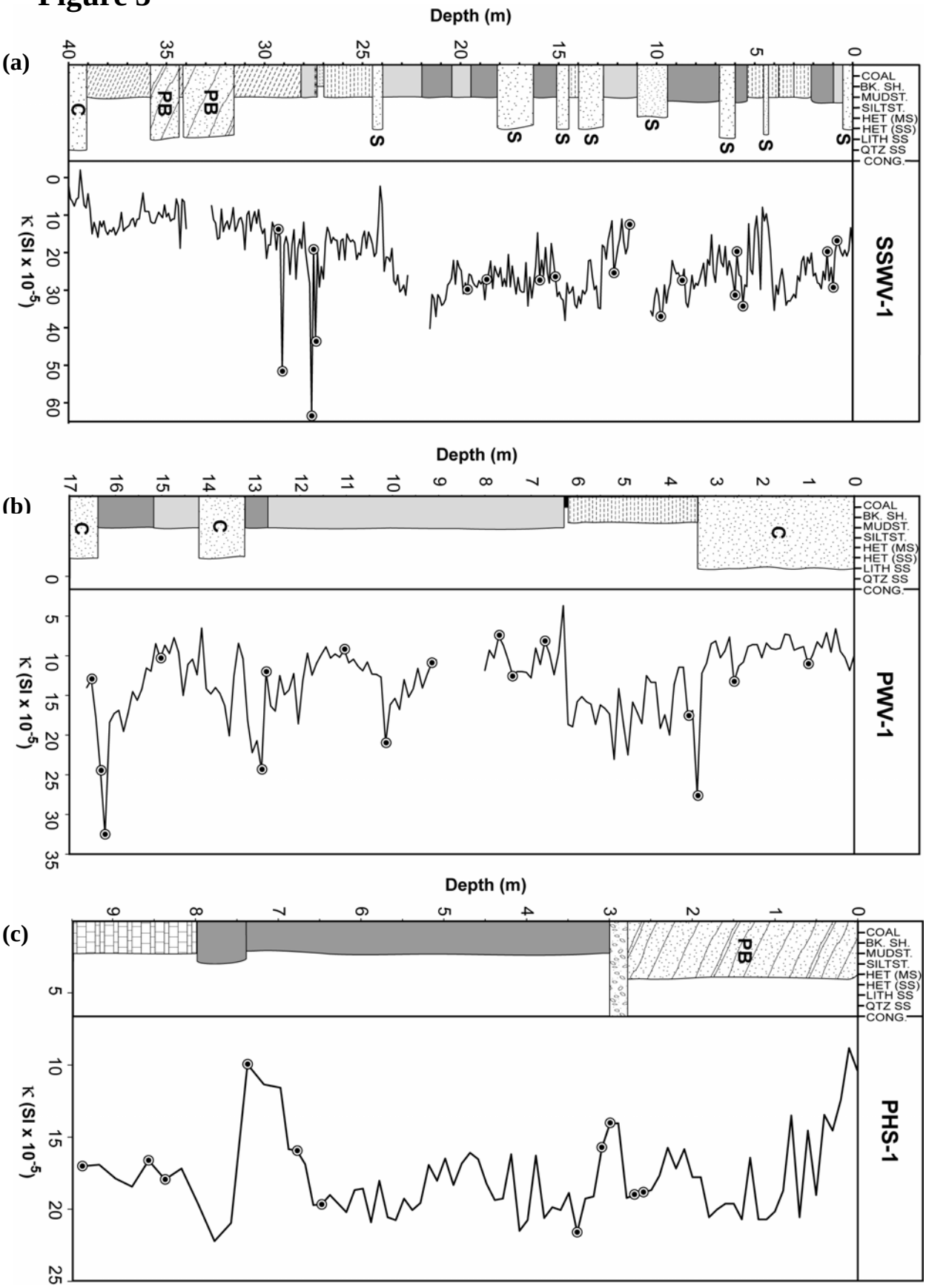
(a)
Depth (m)
C
PB
PB
S
COAL
BK. SH.
MUDST.
SILTST.
HET (MS)
HET (SS)
LITH SS
QTZ SS
CONG.
κ (SI x 10-5)
SSWV-1
(b)
Depth (m)
C
C
C
PWV-1
(c)
Depth (m)
PB
PHS-1

Figure 5

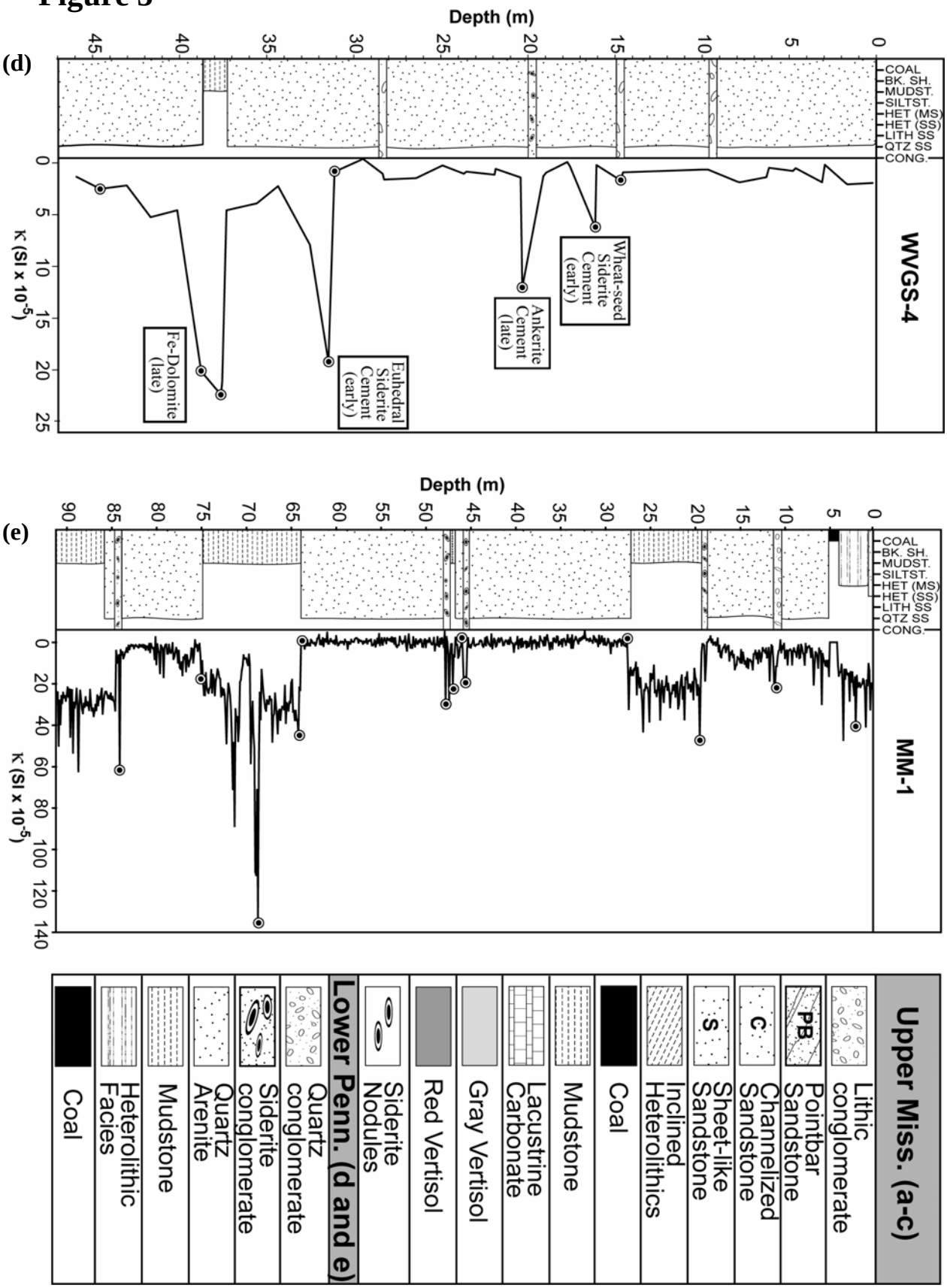
(d)
Depth (m)
COAL
BK. SH.
MUDST.
SILTST.
HET (MS)
HET (SS)
LITH SS
QTZ SS
CONG.
WVGS-4
κ (SI x 10-5)
Wheat-seed Siderite Cement (early)
Ankerite Cement (late)
Euhedral Siderite Cement (early)
Fe-Dolomite (late)
(e)
Depth (m)
MM-1
κ (SI x 10-5)
Upper Miss. (a-c)
Lithic conglomerate
PB
Pointbar Sandstone
C
Channelized Sandstone
S
Sheet-like Sandstone
Inclined Heterolithics
Coal
Mudstone
Lacustrine Carbonate
Gray Vertisol
Red Vertisol
Siderite Nodules
Lower Penn. (d and e)
Quartz conglomerate
Siderite conglomerate
Quartz Arenite
Mudstone
Heterolithic Facies
Coal

Figure 5 - Lithologies and magnetic susceptibility measurements from upper Mississippian outcrops (a-c) and lower Pennsylvanian cores (d and e). Bulls-eyed circles (◉) demarcate samples selected for detailed magnetic analysis. Cement types determined by Reed et al. (2005) are shown in Figure 5d.

Upper Mississippian Continental Facies

Geological Background

Upper Mississippian strata in the study area consist of red and green mudrocks and interbedded sandstones that were deposited in terrestrial and coastal environments (Miller and Eriksson, 2000; Beuthin and Blake, 2002). Miller and Eriksson (2000) recognized five sequence types in the upper Mississippian Mauch Chunk Group outcrop belt in West Virginia: (1) major incised valley fill to coastal plain, (2) major incised valley fill to deltaic, (3) minor incised valley fill, (4) coastal plain/flood plain, and (5) marine-dominated sequences. These authors attribute

Figure 6

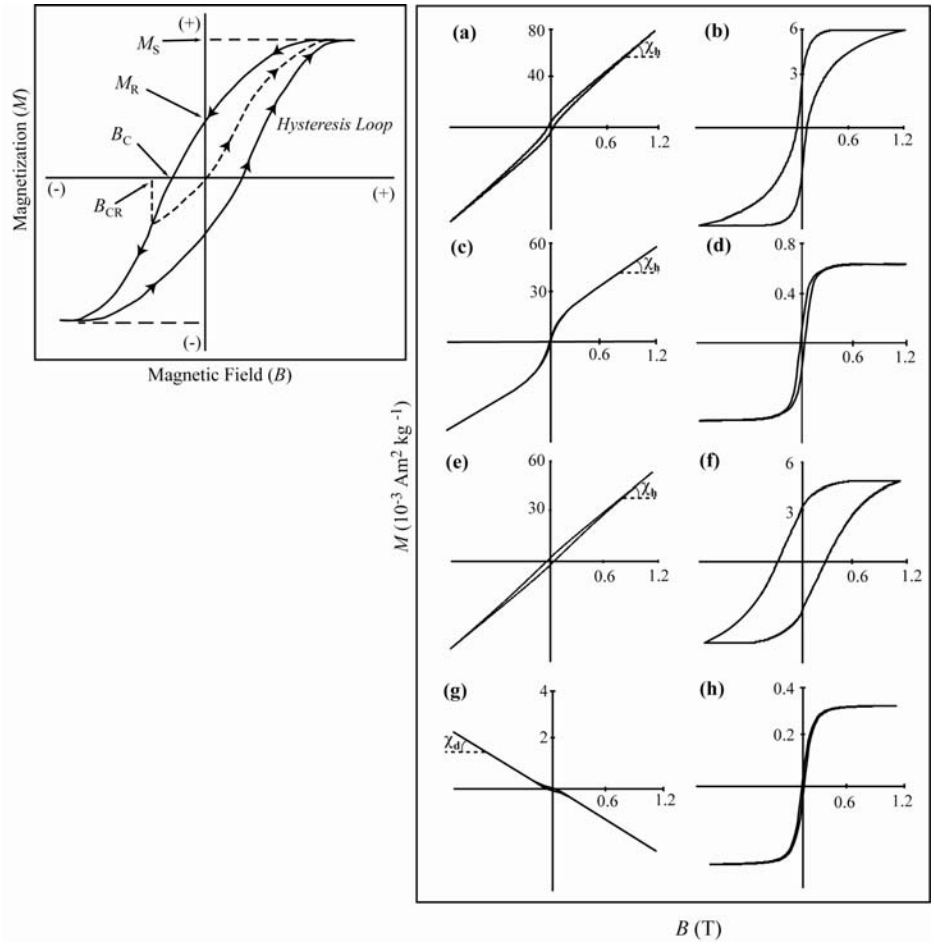

Figure 6 - Examples of hysteresis loops uncorrected (to left) and corrected for paramagnetic or diamagnetic influence (to the right) for upper Mississippian and lower Pennsylvanian facies. (a) paramagnetic, ferrimagnetic, and antiferromagnetic; (b) wasp-waisted ferrimagnetic and antiferromagnetic; (c) paramagnetic and ferrimagnetic; (c) paramagnetic and ferrimagnetic; (d) ferrimagnetic; (e) antiferromagnetic and paramagnetic; (f) antiferromagnetic; (g) diamagnetic and ferrimagnetic; (h) ferrimagnetic loop. The high-field susceptibility (χ_f) and the diamagnetic susceptibility (χ_d) are equivalent to the slope of the closed uncorrected hysteresis loops above 0.8 T. Inset shows the key hysteresis parameters used in the study.

the cyclostratigraphy of these strata to fourth-order glacio-eustasy. Lowstand and transgressive systems tracts consist of incised valleys infilled dominantly by tidal rhythmites. Highstand systems tracts are dominated by floodplain siltstones and mudstones that have been in part pedogenically transformed into red vertisols and rare calcisols (cf. Kraus and Bown, 1988). Tops of some of the highstand systems tract deposits are characterized by thinner, gray to gray-white paleosols and coaly zones that developed as floodplain sediments became water-logged due to a relatively high water table (Miller and Eriksson, 1999; Miller and Eriksson, 2000).

Of particular interest to this study are coastal plain/flood plain sequences consisting of sandstones, mudstones, red and gray vertisols, inclined heterolithic units, and lacustrine carbonates. Figures 5a, b, and c illustrate the vertical succession of lithofacies in the three measured sections, together with volume magnetic susceptibility (?) profiles. It is clear from these profiles that magnetic patterns and anomalies exist within and between lithofacies. Individual lithofacies shown of the Figures 5a, b and c are discussed below.

Lithofacies A: Sandstone Facies

Sandstone facies consist of fine- to medium-grained lithic arenites. These sandstones occur as lenticular channel-shaped bodies (C), inclined, lateral accretion, point-bar deposits (PB), and non-channelized sheet-like bodies (S). Channel bodies range from 1 to 3.5 m thick and from several to 50 m wide and erosionally truncate underlying floodplain facies. Channel fills are typically thin laminated (1-5 cm) with plane bedding and rare low-angle trough cross-beds. Internal fill patterns are typically upward-fining with rare occurrences of basal conglomerates that consist of locally derived siltstone and mudstone clasts (Miller and Eriksson, 2000). Inclined, lateral-accretion point-bar deposits consist of a ~10 cm basal conglomeratic channel lag that truncates underlying red vertisol facies. The basal conglomerate consists of small pebbles of

dark gray, rounded, pedogenic calcareous nodules, minor red mudstone and siltstone intraclasts, Fe-oxide-rich argillaceous nodules, black rolled vertebrate bones, plant material and feldspar grains in a fine-grained sandstone matrix (Turner and Eriksson, 1999). Overlying point-bar deposits are 3-4 m thick and consist of alternating sandstone and mudstone facies. The sandstone facies occur in beds up to 8 cm thick and consist of maroon-red, very fine- to fine-grained sand-size particles. Sedimentary structures include small-scale current ripple cross lamination and carbonaceous plant debris (Turner and Eriksson, 1999). Mudstone beds up to 25 cm thick, are typically silty and structureless but form weakly developed soil structures with shallow root structures near the top of the deposit. Nonchannelized, sheet-like deposits are dark gray to red with rare red siltstone/mudstone intraclasts incorporated along the base. These deposits are tabular and range from 1 to 3 m in thickness and are continuous laterally for hundreds of meters. Where outcrop conditions permit, these tabular sandstone facies can be traced laterally into channel bodies.

Miller and Eriksson (2000) interpret the channelized sandstone bodies as trunk and tributary channel deposits of low-sinuosity fluvial systems. They suggest that fluctuations in relative seal-level may have triggered channel incision into flood-plain facies. Turner and Eriksson (1999) interpret the lateral accretion facies as the deposits of small laterally migrating, relatively shallow, meandering channels that occupied part of a dry coastal alluvial plain. These authors also indicate that the sandstone-mudstone couplets formed during individual flood events where each couplet records rising-flood-stage erosion followed by falling-stage deposition of silt and clay. The non-channelized sandstone bodies are comparable to the early Carboniferous floodplain deposits of South Wales that were interpreted by Wright and Robinson (1988) as crevasse splay deposits related to over-bank flooding.

***Lithofacies B: Gray Mudstone** Facies*

Gray mudstone facies consist of clay- to silt-sized particles within tabular units up to 4 m thick. Beds range in thickness from less than 1 cm to 3 cm and are typically tabular. Rare, localized calcic zones are defined by irregular to concentric shaped siderite nodules that are parallel to bedding planes (Miller and Eriksson, 2000).

The gray mudstones are thought to be relicts of seasonal suspension sedimentation on overbank flood-plains on a low-relief landscape (Miller and Eriksson, 2000). Siderite nodules are

thought to reflect either evolving chemical conditions during progressive burial diagenesis (e.g. Bailey et al., 1998) or the reduction of ferric oxyhydroxides by organic matter (e.g. Postma, 1982) under hydromorphic conditions.

Lithofacies C: Gray Vertisol Facies

Gray vertisol facies consist of clay and silt-rich mudstones that occur as single and stacked tabular paleosols in beds up to 6 m thick. Pedogenic fabrics include platy to angular blocky textures, clay coatings, and well-developed randomly oriented slickensides. Drab-haloed root traces are preserved in platy and blocky textured ped fabrics, and display single and bifurcating patterns. Lycopod impressions occur in the upper section of one gray vertisol. Thin discontinuous calcite zones (~2 cm) defined by irregularly shaped carbonate nodules up to 3 cm in length occur along the base of some gray paleosol facies (Miller and Eriksson, 1997, 2000).

Pedogenic slickensides are the most prominent diagnostic feature in vertic paleosols in the Appalachian Basin (Driese and Mora, 1993). These authors suggest that vertic structures developed in the upper clay-rich parts of fining-upward sequences deposited by high sinuosity, single-channel forms in coastal alluvial plain settings. Field characteristics indicate that the slickensides are randomly oriented, suggesting that they are of non-tectonic origin. Driese and Mora (1993) also suggest that the peds developed by differential shearing to form angular blocky aggregates that are attributed to frequent wetting and drying cycles.

The origin and significance of the gray gleyed to gray-white paleosols and associated coaly zones in the upper Mississippian of southern West Virginia is a subject of debate. Miller and Eriksson (1999) argued that the leached paleosols and coals that cap terrestrial highstand facies developed during wetter, less seasonal climates associated with periods of eustatic fall and lowstand. The shift to more hydromorphic (everwet) conditions was considered to be a response to increases in global ice cover that resulted in a narrowing of the inter-tropical convergence zone and weakening of the monsoonal circulation systems to produce warmer and wetter climatic conditions. In contrast, Beuthin and Blake (2002) attributed gleying in the paleosols to a rising water table and proposed that the development of thin coal beds was fostered by the accumulation of organic material in localized wet areas.

Lithofacies D: Red Vertisol Facies

Red vertisol facies are developed in clayey to sandy mudstone deposits that occur as single and stacked tabular paleosols in beds up to 4 m thick. Pedogenic fabrics include angular blocky textures, clay coatings, and well-developed randomly oriented slickensides. Downward-branching root traces are preserved in the upper sections in many of the red paleosols. Some root traces exhibit either drab reduction haloes or completely reduced rhizoliths. Pedogenic slickensides decrease in size as grain-size increases from clayey to sandy mudstones. In most cases, soil development has disrupted the primary depositional fabrics such that bedding planes cannot be identified.

Retallack (1988) suggests that red coloration, blocky soil textures, clay coatings and pedogenic slickensides reflect seasonal wetting and drying of a well-drained clay-rich soil. These characteristics are ubiquitous throughout the red vertisol facies and likely represent a similar mode of formation to those suggested by Retallack (1988). The stacked nature of these red paleosol facies suggest that repeated episodes of soil development occurred. This interpretation is analogous to that of Kraus and Bown (1988) in which stacked paleosols indicate prolonged periods of pedogenesis on a distal floodplain.

The origin of hematite within the red vertisol facies remains problematic. Dunlop and Ozdemir (1997) argue that hematite pigment in red beds may form via the dehydration of goethite, the inversion of maghemite, or by the oxidation of magnetite:

$$2\alpha FeOOH \rightarrow \alpha Fe_2O_3 + H_2O$$

$$\gamma Fe_2O_3 \rightarrow \alpha Fe_2O_3$$

$$2Fe_3O_4 + O_2 \rightarrow 3\alpha Fe_2O_3$$

Friedman and Sanders (1978) identified five modes of formation of hematite in red-beds: (1) transport and re-deposition of detrital hematite formed in lateritic, humid-tropical climates by the oxidation of ferrous iron derived from ferromagnesian silicate minerals (e.g. pyroxene, hornblende, biotite, and chlorite); (2) *in situ* oxidation of ferrous iron in iron-bearing minerals in previously deposited non-red sediments (e.g. ferromagnesian silicates and magnetite) to brownish hydrated iron oxides that transform to hematite; (3) recrystallization of yellowish and brownish hydrated ferric oxides to hematite that was transported and incorporated into sediments as detrital grains; (4) inheritance from pre-existing red-beds and re-deposition as second-cycle particles; and (5) precipitation directly from sea water during the initial stages of evaporation.

Lateritic soils form as a result of intense subaerial chemical weathering under humid-tropical and subtropical climates. As a result of intense weathering, most of the primary minerals are dissolved and transformed into secondary mineral assemblages, mainly kaolinite, gibbsite, goethite, hematite, and quartz (Theveniaut and Freyssinet, 1999; Price et al., 1997). Upper Mississippian strata in the central Appalachians generally developed under semi-arid to seasonal conditions (Cecil, 1990; Beauthin and Blake, 2002). Therefore, conditions necessary for development of lateritic soil profiles were unlikely to have existed. The fifth proposed mechanism of hematite, precipitating from sea water, is not applicable to these rocks for the reason that these red beds are floodplain sediments that were deposited on a low-lying coastal plain devoid of marine influence.

The second, third and fourth modes of formation for hematite in red-beds are favored here for the reason that the upper Mississippian climate was seasonally wet and could likely produce and oxidize ferric oxides and hydroxides to hematite. Moreover, recycled red mudstone and siltstone clasts present in many lag deposits (e.g. basal point-bar deposits) have been interpreted as second-cycle hematite-rich sediments. Similar studies indicate that *in situ* reddening of detrital ferric hydroxides in clay-rich sediments is promoted by seasonal lowering of water tables and development of well-drained oxygenated conditions that allow the oxidation of organic matter and eventual development of hematite (Burley et al., 1985).

Lithofacies E: Limestone Facies

Limestone facies consist of yellow to gray laminated (1 to 3 cm) lime mudstones that occur in 1.5 m thick tabular beds. This facies is intercalated with terrigenous red mudrocks and persists laterally for hundreds of meters. Dense micrite with a weak laminar or peloidal fabric and sparse ostracods and bivalves have been identified in thin section (Miller and Eriksson, 2000). Platt and Wright (1991) interpret similar carbonate beds as coastal or playa deposits that developed during shallow floodplain inundation.

Lower Pennsylvanian Incised-Valley-Fill Facies

Geological Background

The New River Formation has been grouped into two main facies belts: a western belt dominated by thick (~70 meters) tabular (up to 90 km wide, ~500 km long) quartz arenites grading upwards into heterolithic facies and dark mudstone-sandstone, and an eastern belt dominated by shale, siltstone, coal, and discontinuous lithic sandstone bodies (Korus, 2002). Lithologies in the eastern facies belt are interpreted as fluvio-deltaic deposits derived from the fold-and-thrust belt to the southeast (Englund and Thomas, 1990). In contrast, lithologies in the western facies belt are interpreted as the deposits of braided-alluvial trunk river systems that flowed down the axis of the foreland basin (Korus, 2002). Furthermore, outcrop analyses of equivalent facies in Kentucky and southwest Virgina reveal that the western quartz arenite belts consist of multistory, sheet-form, and channel-from elements (Greb et al., 2004). These authors point out that pairs of composite sandstones in each quartz arenite belt occur along similar trends and are separated by a mid-formation shale that possibly represents a genetic-sequence boundary at its base. Heterolithic and dark mudstone facies that cap the major sandstone bodies are interpreted as tidal estuarine deposits related to transgressive drowning of the braid plain (Korus, 2002).

Of particular interest to this study are the quartz arenites and associated heterolithic facies of the western belt. Figures 5d and e illustrate the associations of lithofacies and volume magnetic susceptibility (κ) profiles. It is clear from the magnetic patterns that anomalies exist within and between lithofacies. Individual lithofacies shown on Figures 5d and e are discussed below.

Lithofacies F: Quartz Arenite Facies

Quartz arenite facies make up intervals of amalgamated sandstones up to 40 m thick. Typical facies consist of coarse- to fine-grained sandstone with local quartz- and siderite-pebble conglomerate lags that define reactivation surfaces indicative of multi-story channel fills. In outcrop, Korus (2002) recognized a four-fold hierarchy of bounding surfaces within these sandstone bodies in which upward-thinning, medium- to large-scale tabular and trough cross-bed sets, plane bed, sand ripple cross strata are superimposed on gently inclined surfaces. This author

also suggests that deposition occurred via bedform migration over sandy, downstream accreting macroforms and, to a lesser extent, laterally accreting macroforms.

Detrital grains are generally well sorted and well rounded mono- and polycrystalline quartz. Detailed diagenetic studies have been conducted on core WVGS-4 by Reed et al. (2005). Quartz is the most common cement and generally occurs as syntaxial overgrowths; however less abundant prismatic quartz crystals protrude into secondary pore spaces. Fe-oxides/oxyhydroxides are common and occur as thin, early coatings on primary grains. Reed et al. (2005) propose that the presence of oxidized Fe-bearing minerals implies communication with atmospheric oxygen. Calcite is the second most common cement type and occurs as large inter-granular crystals in compositionally mature coarse-grained samples (Reed et al., 2005). Siderite ($FeCO_3$), the third most common cement type, is an authigenic iron-bearing carbonate common in many diverse sedimentary settings (Pan et al., 2000). This cement occurs as small (< 20 μm) euhedral crystals surrounding detrital grains (predominantly quartz) and as "wheat-seed" siderite (Reed et al., 2005). In contrast to the early Fe-oxide grain coats in the quartz-cemented arenites, siderite cements are indicative of reducing pore fluids.

Fe-dolomite and ankerite cements are present in some samples and generally occur as a replacement of earlier calcite cements (Reed et al., 2005). Based on textural evidence, these authors indicate that Fe-dolomite and ankerite cements formed during deep burial after the formation of secondary porosity. Fe-rich fluids introduced from tectonic highlands and clay mineral transformations in surrounding shales are two proposed sources for late diagenetic Fe in the Appalachian Basin (Reed et al., 2005).

Lithofacies G: Heterolithic Facies

Heterolithic facies consist of a 4 m-thick interval of thinly interlaminated shale, siltstone and fine-grained sandstone. In outcrop, sedimentary structures consist of lenticular, wavy, and flaser bedding, ripple cross laminae, and trough cross bedding (Korus, 2002). In core samples, wavy and ripple laminated bed sets become more apparent up section. Rhythmic bundles are crude near the base of the succession, but become more obvious and distinguishable up section, and occur as 1-2 cm-thick interlayered sandstone-rich and mudstone-rich beds in which sandstone laminations display thickening and thinning trends.

The thickening and thinning patterns are commonly interpreted as the result of variations in tidal velocities from spring to neap tides (Kvale et al., 1989; Kvale et al., 1995; Miller and Eriksson, 1997). Moreover, the occurrence of wavy and ripple laminated beds up section are suggestive of alternating current flow and slack water periods (Reineck and Wunderlich, 1968; cf. Korus, 2002).

Lithofacies H: Dark Mudstone-Sandstone Facies

These facies largely consist of upward-coarsening, 1.5 to 12 m-thick units of mudstone, siltstone, and very-fine sandstone. Sedimentary structures include lenticular and wavy bedding, and ripple cross-laminae. In general, bedding changes upwards from planar to rippled within a single coarsening upward interval. Cross-bedded sandstone lenses are common near the tops of these units. Korus (2002) found that the average thickness of individual upward-coarsening units varies with geographic location and stratigraphic position. In the northwestern areas, units above the Upper Raleigh Sandstone are relatively thin (1.5 – 2 m), whereas in southeastern areas the same stratigraphic interval contains thicker (6 – 9 m) upward-coarsening units. This author suggests that these facies represent progradational deltaic complexes and argues that the thin coarsening-upward successions were formed by prograding bayhead deltas and estuary mouth bars during the early infilling of estuaries, whereas thicker coarsening-upward successions were formed as prograding deltaic complexes.

Magnetic Characteristics

Lithofacies A: Sandstone Facies

Sandstones sampled from upper Mississippian outcrops consist of multiple magnetic mineral types. The SSWV-1 sheet-like sandstones (Fig. 5a) primarily contain paramagnetic (e.g. siderite), antiferromagnetic (e.g. hematite) and ferrimagnetic (e.g. magnetite) minerals as indicated by hysteresis loop shapes (Figs. 6a and b). Antiferromagnetic signatures are indicated by high B_{CR} values (Fig. 7). The Day Plot (Fig. 8) shows that these samples are also associated with high magnetization ratios (M_{RS}/M_s) compared to other upper Mississippian sandstone samples. This is attributed to the influence of hematite, an antiferromagnetic mineral generally

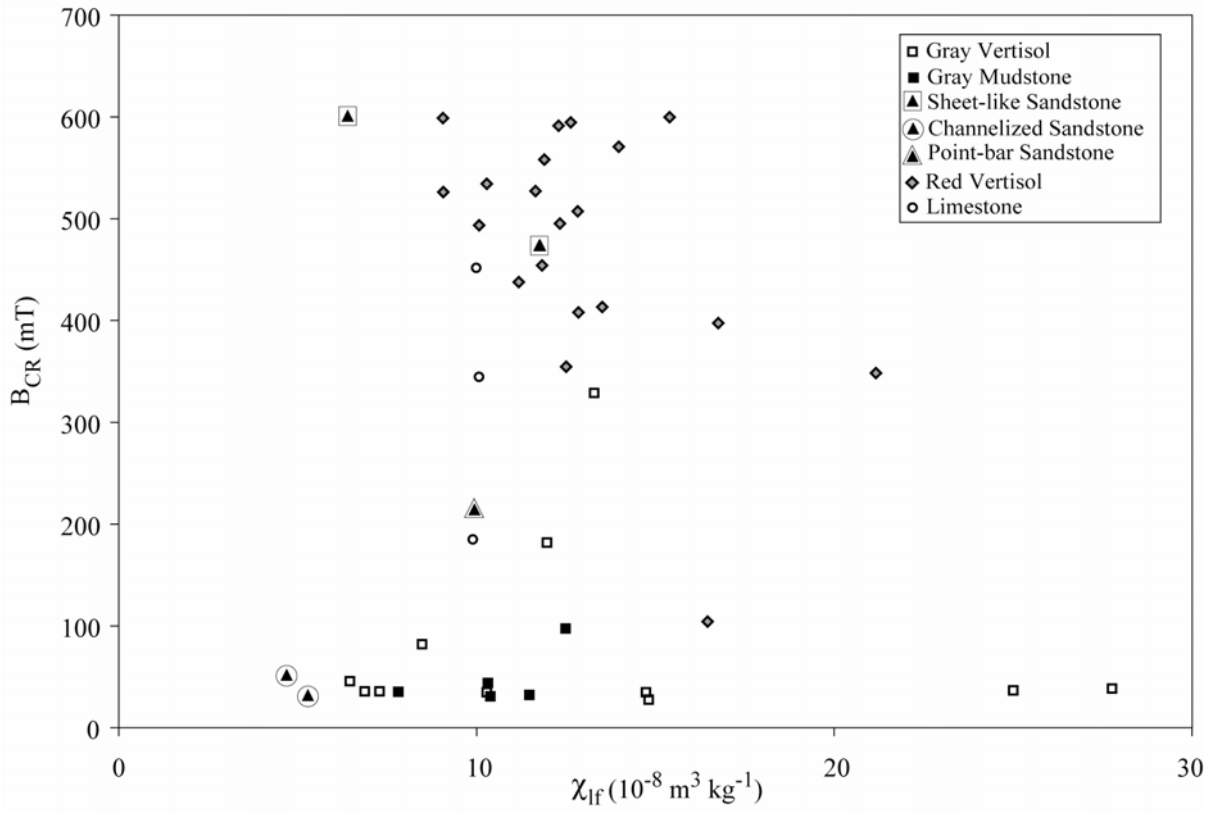

Figure 7 - Coercivity of remanence (B_{CR}) vs. low-frequency mass magnetic susceptibility (χ_{lf}) for upper Mississippian samples. High B_{CR} values (>300 mT) correspond to samples with hematite whereas low B_{CR} values (<60 mT) correspond to samples with magnetite. Samples falling between these values contain titanomagnetite or represent complex mixtures of magnetite/titanomagnetite and hematite.

associated with much higher magnetization ratios, compared to ferrimagnetic minerals like magnetite, titanomagnetite and maghemite (Peters and Dekkers, 2003). Mean high-field susceptibility (χ_h mean = 3.9×10^{-8} m^3 kg^{-1}) and ferrimagnetic susceptibility (χ_{ferri} mean = 3.8×10^{-8} m^3 kg^{-1}) values (Fig. 9) indicate that χ_{lf} values represent virtually equivalent contributions from the ferrimagnetic and additive antiferromagnetic + paramagnetic mineral phases. M_S data (Fig. 10) indicate that paramagnetic minerals are higher in concentration compared to ferrimagnetic and antiferromagnetic minerals. In order to have equivalent χ_h and χ_{ferri} values, the antiferromagnetic concentration must be greater than the ferrimagnetic concentration, or the paramagnetic mineral type and concentration are sufficient to raise χ_h in conjunction with the antiferromagnetic mineral phase influences. Magnetic characteristics of the sheet-like

sandstones, particularly wasp-waisted loops trends, imply the presence of both magnetite/titanomagnetite and hematite in these sandstones.

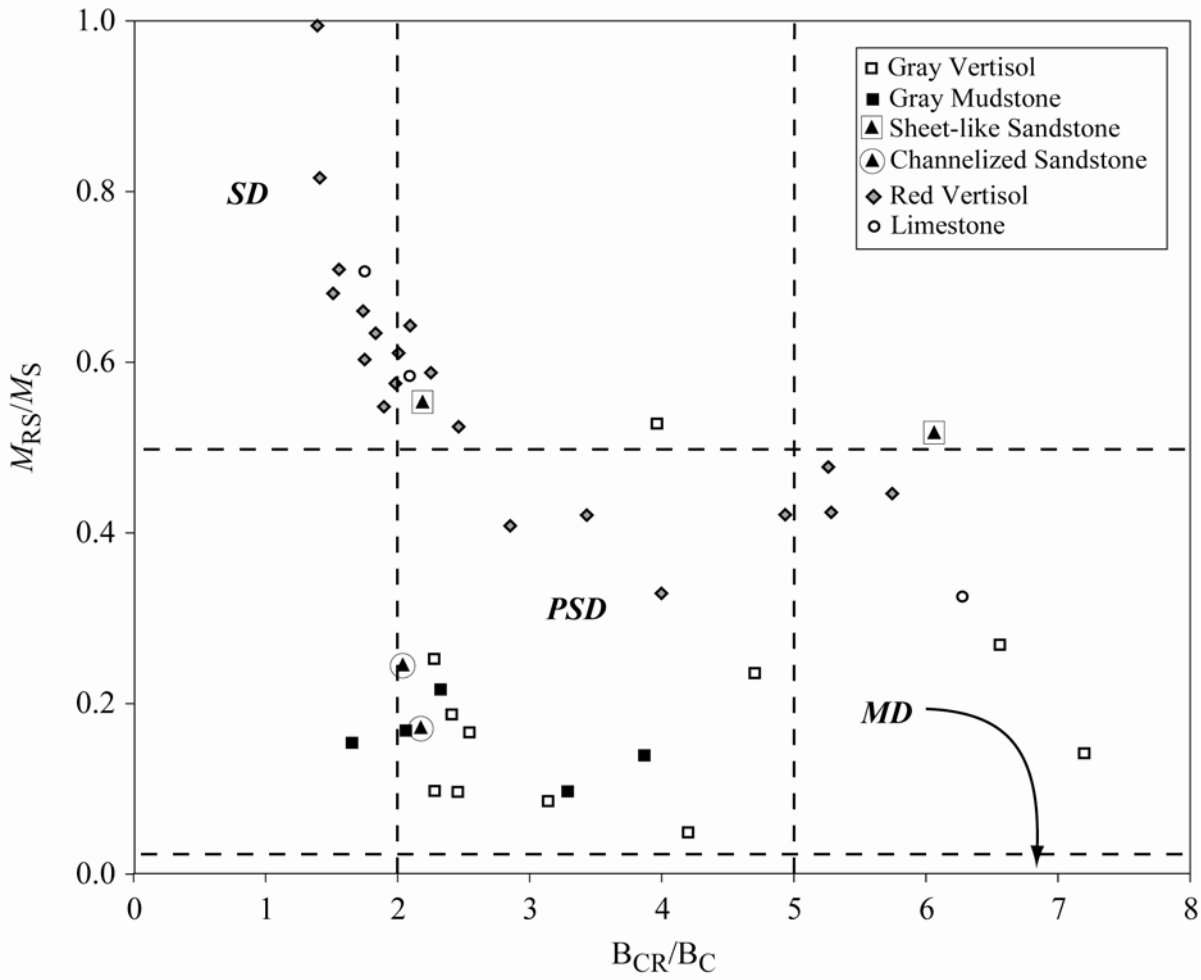

Figure 8 - Day Plot illustrating the effects of mineralogy and grain-size variations as a function of hysteresis ratios for upper Mississippian samples. Hematite influenced samples are associated with higher magnetization ratios (M_{RS}/M_S). Single domain (SD), pseudo-single domain (PSD), and multidomain (MD) fields after Dunlop and Ozdemir (1997) apply only to samples in which magnetite has been identified

In contrast to the SSWV-1 sheet-like sandstones, the PWV-1 channelized sandstones (Fig. 5b) primarily consist of paramagnetic and ferrimagnetic (magnetite) minerals as indicated by hysteresis loop shapes (Figs. 6c and d) and low B_{CR} values (Fig. 7). Figure 7 indicates that these samples are also characterized by low magnetic susceptibility (χ_{lf} mean = 5.0×10^{-8} m^3 kg^{-1}). The low χ_{lf} values imply that magnetite exists in limited concentration. The Day plot (Fig. 8)

indicates that these samples have low magnetization ratios compared to the other upper Mississippian sandstone samples, and fall in the PSD field for magnetite. χ_h (χ_h mean = 4.8×10^{-8} m^3 kg^{-1}) and χ_{ferri} (χ_{ferri} mean = 0.2×10^{-8} m^3 kg^{-1}) values (Fig. 9), reveal that paramagnetic minerals are the dominant contributors to χ_{lf} since $\chi_h > \chi_{ferri}$. Furthermore, M_S data (Fig. 10) show that paramagnetic minerals are higher in concentration compared to ferrimagnetic minerals.

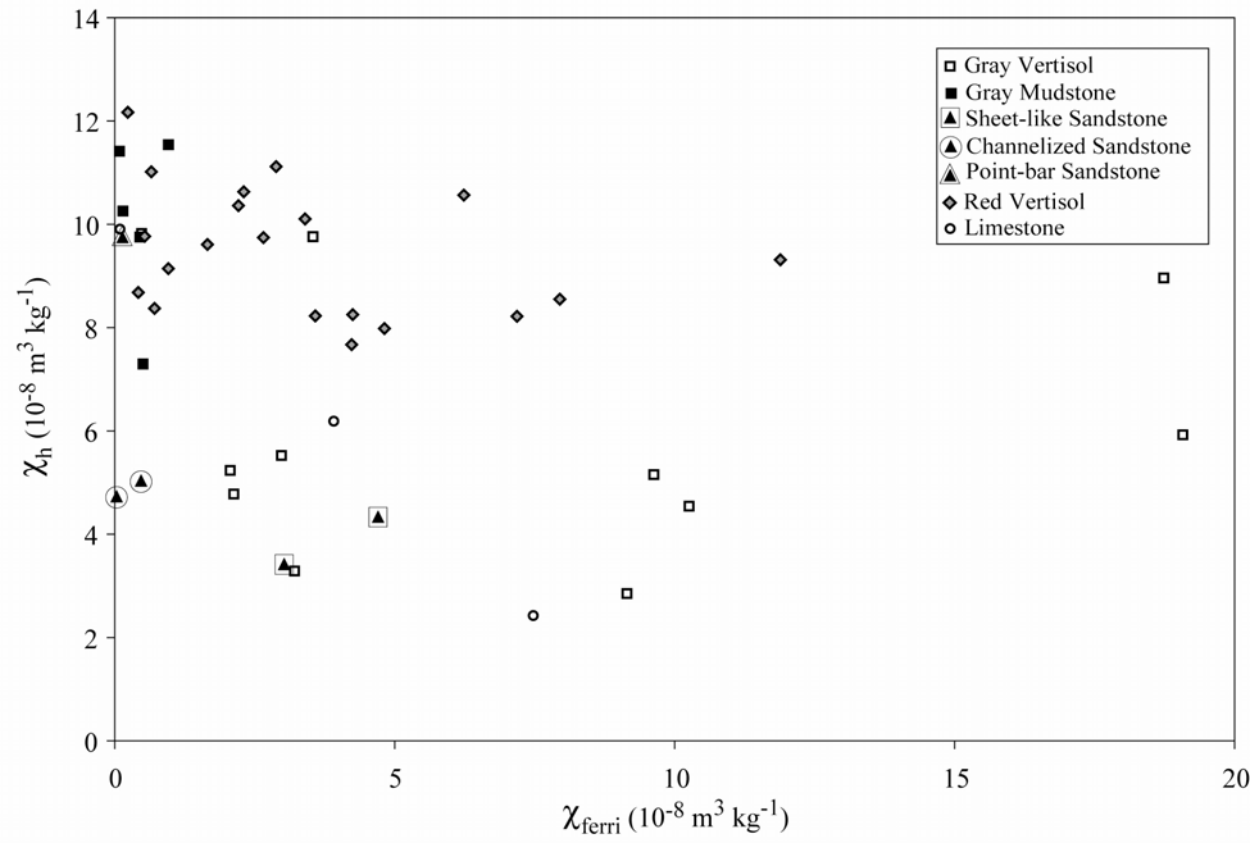

Figure 9 - Ferrimagnetic susceptibility (χ_{ferri}) vs. paramagnetic susceptibility (χ_h) for upper Mississippian samples. χ_h = high-field (> 0.8 T) slope of hysteresis loop and is equivalent to the paramagnetic + antiferromagnetic contribution to χ_{lf}. $\chi_{ferri} = \chi_{lf} - \chi_h$ and is equivalent to the ferrimagnetic contribution to χ_{lf}. In samples with no antiferromagnetic minerals (e.g. hematite), χ_h is equivalent to the paramagnetic contribution to χ_{lf}.

These relationships suggest that the magnetic susceptibility of these samples is primarily controlled by the concentration of paramagnetic minerals and, further, indicates that the magnetite concentration is particularly low in these samples.

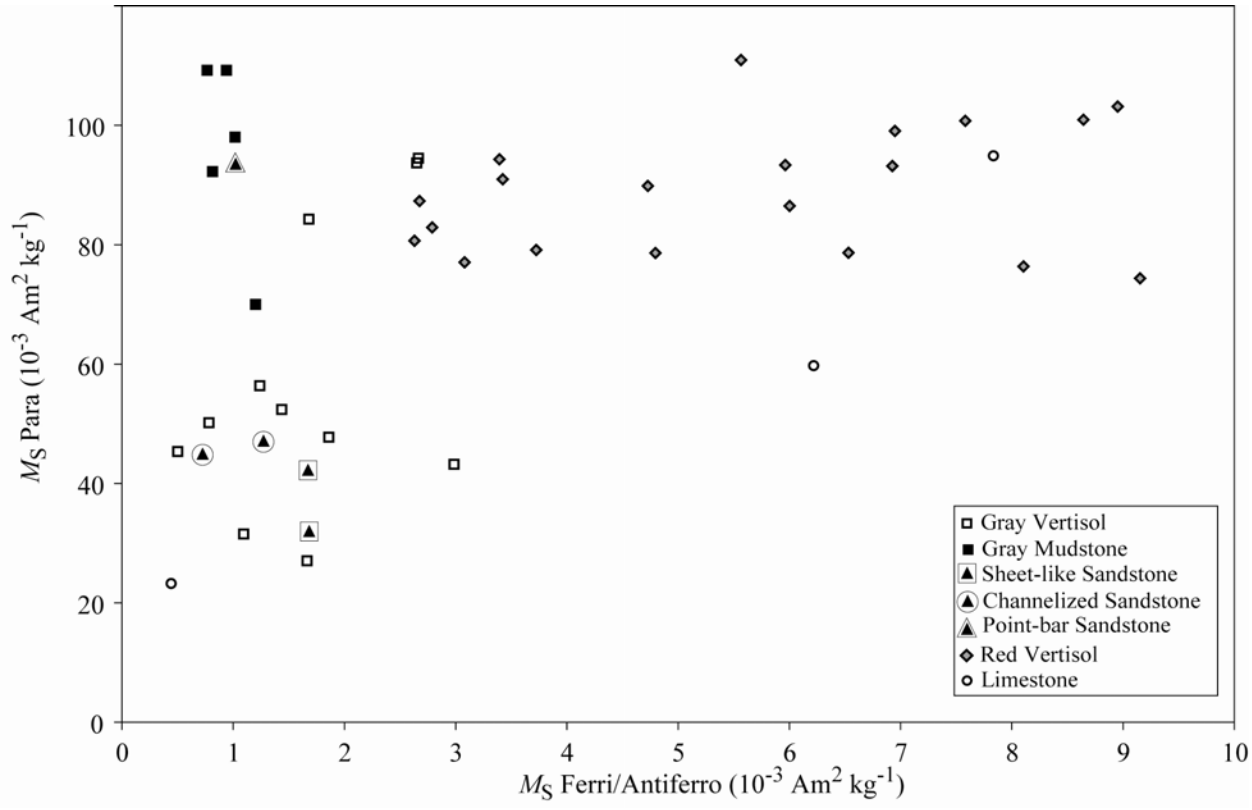

Figure 10 - Paramagnetic M_S vs. Ferri/antiferromagnetic M_S for upper Mississippian samples. M_S is a concentration-dependent parameter that increases monotonically with the amount of magnetic material present. M_s Para refers to the paramagnetic M_S (paramagnetic concentration) obtained from uncorrected hysteresis loops. M_S ferri/antiferro reflects either ferrimagnetic M_S in samples lacking antiferromagnetic minerals (e.g. hematite), or antiferromagnetic M_S in samples lacking ferrimagnetic minerals (e.g. magnetite and titanomagnetite), or the combined antiferromagnetic M_S + ferrimagnetic M_S in samples associated with both ferrimagnetic and antiferromagnetic minerals (e.g. wasp-waisted hysteresis loops indicating mixtures of magnetite and hematite).

The PHS-1 point-bar sandstone sample (Fig. 5c) contains a mixture of paramagnetic and ferrimagnetic minerals as indicated by hysteresis loops (Figs. 6c and d). However, elevated B_{CR} values indicate that another higher-coercivity mineral phase (e.g. titanomagnetite) is also present. The hysteresis loop of the sample does not display any discernable evidence for antiferromagnetic (hematite) contributions such as open loop above fields of 0.4 T or wasp-waistedness (Figs. 7a and b). Figure 7 indicates that this sample is associated with a moderate B_{CR} value (B_{CR} = 155 mT) compared to the high B_{CR} sheet-like sandstones and low B_{CR} channelized sandstones. Due to an anomalously high coercivity ratio (B_{CR}/B_C = 17.6), this sandstone sample is not plotted on Figure 8. The high B_{CR}/B_C value implies that higher

coercivity minerals (e.g. SD magnetite or titanomagnetite) are contributing to the remanence of the sample. The associated low M_{RS}/M_S ratio ($M_{RS}/M_S = 0.13$) suggests that SD grains are not responsible for the higher coercivity phase. SD influence would be expected to have a higher M_{RS}/M_S ratio for the reason that SD grains are too small to reduce their magnetostatic energy (see Appendix A) by forming domain walls. As a result, SD grains have higher M_{RS} values since they are harder to demagnetize. Therefore, coarse PSD and possibly MD titanomagnetite particles are a likely source for the high B_{CR}/B_C and low M_{RS}/M_S ratios.

Peters and Dekkers (2003) compiled a data set of magnetic parameters from a number of publications for several common iron oxide phases. Values for our sample ($B_{CR} = 155$ mT, $B_{CR}/B_C = 17.6$, and $M_{RS}/M_S = 0.14$) best match titanomagnetite for which Peters and Dekkers (2003) list B_{CR} values ranging from 8.5 to 213 mT, B_{CR}/B_C values from 1.2 to 6.9, and M_{RS}/M_S values from 0.01 to 0.53. Therefore, titanomagnetite is probably the dominant remanence carrier in the point-bar sandstones. High-field susceptibility ($\chi_h = 9.8 \times 10^{-8}$ m^3 kg^{-1}) and ferrimagnetic susceptibility ($\chi_{ferri} = 0.2 \times 10^{-8}$ m^3 kg^{-1}) values for the point-bar sandstone indicate that paramagnetic minerals are the dominant contributors to χ_{lf} since $\chi_h > \chi_{ferri}$ (Fig. 9). M_S data (Fig. 10) show that paramagnetic minerals are higher in concentration compared to ferrimagnetic minerals (titanomagnetite). These relationships suggest that the magnetic susceptibility of this sample is primarily controlled by paramagnetic minerals and to a lesser titanomagnetite.

Lithofacies B: Gray Mudstone Facies

Gray mudstones (Fig. 5a and b) primarily consist of paramagnetic and ferrimagnetic minerals as indicated by hysteresis loop shapes (Figs. 6c and d). Figure 7 indicates that these samples are characterized by low mean χ_{lf} (10.5×10^{-8} m^3 kg^{-1}) and low mean B_{CR} (47.7 mT) values indicative of the mineral magnetite. One sample displays an elevated B_{CR} value (98 mT) that suggests the presence of a higher coercivity mineral phase (e.g. titanomagnetite or hematite). In either case, antiferromagnetic contributions are assumed negligible since the hysteresis loop for the sample does not display any discernable evidence for antiferromagnetic contributions (e.g. open loop above fields of 0.4 T or wasp-waistedness; Figs. 6a and b). This suggests that titanomagnetite, or some other ferrimagnetic mineral may be responsible for the elevated B_{CR} values. Furthermore, the hysteresis parameters for this sample ($B_{CR} = 98$ mT, $B_{CR}/B_C = 3.9$, and $M_{RS}/M_S = 0.14$) best match the Peters and Dekkers (2003) values for titanomagnetite. The Day

Plot (Fig. 8) indicates that the magnetic grain-sizes for these samples primarily fall in the PSD field for magnetite. One sample associated with a lower B_{CR}/B_C ratio falls below the PSD boundary and likely indicates that a bimodal grain-size distribution exists between SD and PSD magnetite grains. Mean χ_h (10.0×10^{-8} m^3 kg^{-1}) and χ_{ferri} (0.4×10^{-8} m^3 kg^{-1}) values (Fig. 9) imply that paramagnetic minerals are the dominant contributors to χ_{lf} since $\chi_h > \chi_{ferri}$. Furthermore, the paramagnetic mineral concentration is greater than the ferrimagnetic concentration as illustrated in Figure 10. These relationships suggest that the magnetic susceptibility of these samples is primarily controlled by paramagnetic minerals, and in particular their concentration.

Lithofacies C: Gray Vertisol Facies

The gray vertisol samples (Figs. 5a and b) primarily consist of paramagnetic and ferrimagnetic minerals as illustrated by hysteresis loop shapes (Fig. 6c and d). However, antiferromagnetic characteristics, attributed to either hematite or titanomagnetite, are present in a few of the gray vertisol samples as indicated by elevated B_{CR} values (Fig. 7). χ_{lf} values (Fig. 7) display a wide range from 6.5 to 27.7×10^{-8} m^3 kg^{-1} (χ_{lf} mean = 13.4×10^{-8} m^3 kg^{-1}). Most of the samples have low B_{CR} values (ranging from 28 to 46 mT; Fig. 7) indicative of magnetite. However, three samples display elevated B_{CR} values (82, 182, and 330 mT) that suggest the presence of higher coercivity mineral phases (e.g. titanomagnetite or hematite). The two higher-coercivity samples have hysteresis loops that are open above fields of 0.4 T and display wasp-waisted characteristics indicative of mixtures of hematite and magnetite (e.g. Fig. 6a and b). However, the lowest of these high-coercivity samples displays ferrimagnetic loop characteristics (e.g. Figs. 6c and d) that suggest the presence of titanomagnetite. This interpretation is supported by the hysteresis parameters (B_{CR} = 82 mT, B_{CR}/B_C = 4.7, and M_{RS}/M_S = 0.24) that best match the Peters and Dekkers (2003) values for titanomagnetite. The Day Plot (Fig. 8) indicates that the magnetic grain size for the magnetite interpreted samples largely fall in the PSD region. One magnetite sample falls above the upper M_{RS}/M_S = 0.5 boundary and may indicate that finer remanence carrying magnetite grains (SD) are mixed with PSD grains. In samples where hematite is identified, high B_{CR}/B_C values (> 6) are observed and indicate that complex grain-to-grain interactions between magnetite and hematite and high-coercivity phases (hematite) are contributing to the remanence of the samples.

Mean χ_h (6.0×10^{-8} m^3 kg^{-1}) and χ_{ferri} (7.4×10^{-8} m^3 kg^{-1}) values (Fig. 9) indicate that, overall, ferrimagnetic minerals are the dominant contributors to χ_{lf} since $\chi_{ferri} > \chi_h$. M_S data (Fig. 10) indicate that paramagnetic minerals are higher in concentration compared to ferrimagnetic minerals. These relationships show that the magnetic susceptibility for most of the samples is controlled by low concentrations of PSD magnetite and high concentrations of paramagnetic minerals. However, for one sample, χ_{lf} is dominated by hematite since $\chi_h > \chi_{ferri}$ (9.8 and 3.5×10^{-8} m^3 kg^{-1}, respectively).

Lithofacies D: Red Vertisol Facies

The vertisol samples (Figs. 5a, b, and c) primarily consist of paramagnetic, antiferromagnetic, and ferrimagnetic minerals as indicated by hysteresis loop shapes (Figs. 6a, b, e and f). Figure 7 shows that large variations in B_{CR} (104 to 600 mT, B_{CR} mean = 475.6 mT) occur over a narrow range of χ_{lf} values (9.1 to 21.2×10^{-8} m^3 kg^{-1}, χ_{lf} mean = 12.9×10^{-8} m^3 kg^{-1}) indicating the strong influence of concentrat ion and grain size on magnetic susceptibility. B_{CR} values in these samples are among the highest observed in the upper Mississippian sample set and indicate the presence of hematite. Furthermore, hysteresis loops for the red vertisols remain open at fields above 0.4 T and largely display wasp-waisted loop patterns (e.g. Fig. 6b) suggesting the presence of both hematite and magnetite. The Day Plot (Fig. 8) indicates that these samples have the highest M_R/M_S ratios (0.33 to 0.99, M_R/M_S mean = 0.58) observed in the upper Mississippian sample set. Mean B_{CR}/B_C ratios are relatively low (2.76) but range from 1.38 to 5.70. High M_R/M_S and low B_{CR}/B_C ratios are characteristic of hematite dominated samples (Peters and Dekkers, 2003).

χ_h and χ_{ferri} values indicate that overall antiferromagnetic and, to a lesser extent, paramagnetic minerals are the dominant contributors to χ_{lf} since $\chi_h > \chi_{ferri}$ (Fig. 9). M_S data (Fig. 10) indicate that paramagnetic minerals are higher in concentration compared to antiferromagnetic minerals. However, the antiferromagnetic concentrations for these samples are among the highest observed in the upper Mississippian sample set. Furthermore, these samples encompass a wide range of antiferromagnetic concentrations in conjunction with high paramagnetic concentrations.

Lithofacies E: Limestone Facies

The Upper Mississippian limestone samples (Fig. 5c) primarily consist of paramagnetic, antiferromagnetic, and ferrimagnetic minerals as indicated by hysteresis loop shapes (Figs. 6a and b). Magnetically, these samples behave in different manners with respect to mineralogy, concentration, and grain-size. Figure 7 shows that relatively large variations in B_{CR} (185 to 451 mT) occur over a narrow range of χ_{lf} values (9.9 to 10.1 x 10^{-8} m^3 kg^{-1}). These B_{CR} values indicate that high coercivity phases (e.g. titanomagnetite and hematite) are present in the samples. Hysteresis loops (e.g. Fig. 6a) display the characteristic antiferromagnetic loop patterns that remain open below fields of 0.4 for the two higher coercivity samples (Fig. 7). These samples also display wasp-waisted loop patterns (e.g. Fig. 6b) indicating the presence of a lower coercivity mineral phase (e.g. titanomagnetite or magnetite). The lowest coercivity limestone sample (Fig. 7) does not display any discernable antiferromagnetic hysteresis loop characteristics. However; the B_{CR} data suggests that a higher coercivity phase is present (e.g. titanomagnetite). The hysteresis parameters for this sample (B_{CR} = 185 mT, B_{CR}/B_C = 6.3, and M_{RS}/M_S = 0.33; Figs. 7 and 8) fall with in the range of the Peters and Dekkers (2003) hysteresis parameters for titanomagnetite. Therefore, the ferrimagnetic component in this limestone sample is likely titanomagnetite. The Day Plot (Fig. 8) shows that two hematite-rich limestone samples with high M_{RS}/M_S ratios plot with the red vertisol samples. The third sample is associated with a lower M_{RS}/M_S ratio and a higher B_{CR}/B_C ratio indicating that more complex grain-grain interactions are occurring in the sample. The high B_{CR}/B_C value indicates that higher coercivity minerals are contributing to the samples remanence and that complex grain-grain interactions are occurring between contrasting coercivity phases.

Figure 9 shows that these samples have very different contributions to χ_{lf}. χ_h values increase with decreasing χ_{ferri} values indicating an increase in hematite and a decrease in magnetite content. Furthermore, in two samples $\chi_h > \chi_{ferri}$ indicate that antiferromagnetic and, to a lesser, paramagnetic minerals have a greater contribution to χ_{lf} compared to the ferrimagnetic contribution. However, in the other sample $\chi_{ferri} > \chi_h$ indicating that ferrimagnetic minerals contribute more to χ_{lf} than antiferromagnetic and paramagnetic minerals. M_S data (Fig. 10) show that paramagnetic minerals are higher in concentration compared to antiferromagnetic and ferrimagnetic minerals. Collectively, these samples encompass a wide range of paramagnetic, antiferromagnetic, and ferrimagnetic concentrations as illustrated in Figure 10.

Lithofacies F: Quartz Arenite Facies

WVGS-4 Samples

Sandstones sampled from WVGS-4 (Figs. 5d) have been separated into quartz-cemented sandstones and Fe-carbonate cemented sandstones based on microprobe analysis (Reed et al., 2005) and multi-parameter magnetic analysis (this study). Quartz-cemented sandstones primarily consist of diamagnetic and ferrimagnetic minerals. Hysteresis loops generally display weak ferrimagnetic loop characteristics below 0.2 mT and diamagnetic loop characteristics above 0.2 mT and (e.g. Fig. 6g). Figure 5d shows that these samples display low κ values (0.9 to 2.6 × 10^{-5} SI) characteristic of quartz-dominated samples. Figure 11 indicates that these samples are associated with relatively low B_{CR} values (47.7 to 76.3 mT) and weak (mostly negative) χ_{lf} values (-0.3 to 1.2 × 10^{-8} m^3 kg^{-1}). Low B_{CR} values suggest that magnetite is the ferrimagnetic

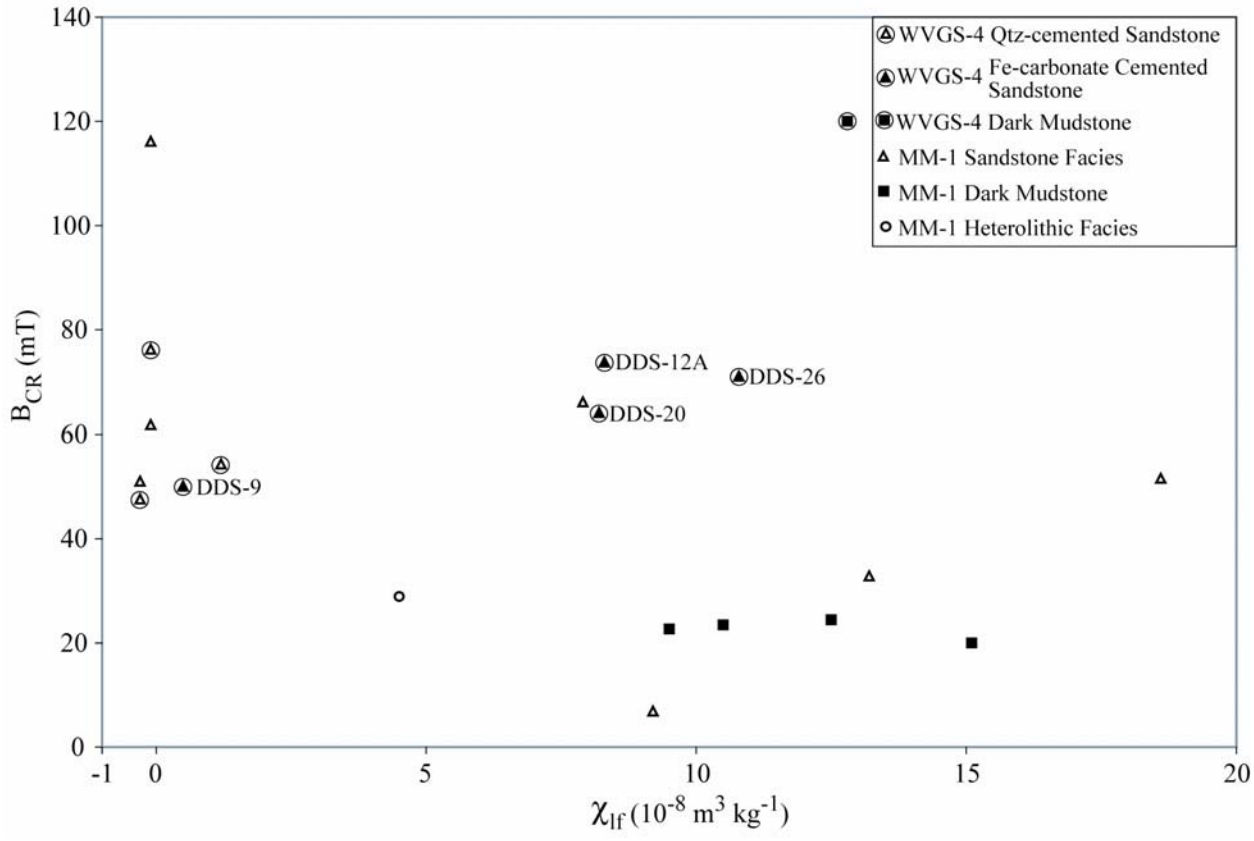

Figure 11 - Coercivity of remanence (B_{CR}) vs. low-frequency mass magnetic susceptibility (χ_{lf}) for lower Pennsylvanian samples. High B_{CR} values (>300 mT) correspond to samples with hematite whereas low B_{CR} values

(<60 mT) correspond to samples with magnetite. Samples falling between these values contain titanomagnetite or represent complex mixtures of magnetite/titanomagnetite and hematite.

contributor. However, higher-coercivity phases (e.g. SD magnetite or titanomagnetite) may be present in the quartz-cemented sample with the higher B_{CR} (76.3 mT) value. The Day Plot (Fig. 12) indicates that the associated magnetic grain-size of these samples fall in the PSD field. Since SD influence is not suggested in Figure 12, and wasp-waisted loop characteristics are not observed in any of the samples, as would be expected for mixtures of high-coercivity SD magnetite and low-coercivity PSD magnetite, the ferrimagnetic phase in the elevated B_{CR} (B_{CR} = 76.3) sample is likely titanomagnetite. Moreover, the hysteresis parameters for this sample (B_{CR} = 76.3 mT, B_{CR}/B_C = 3.6, and M_{RS}/M_S = 0.07) best match the Peters and Dekkers (2003) values for titanomagnetite. These quartz cemented arenites are largely associated with very low χ_h and χ_{ferri} values (Fig. 13) and low paramagnetic M_S and ferrimagnetic M_S values (Fig. 14) indicating that paramagnetic and ferrimagnetic minerals have a minimal contribution to χ_{lf} as a result of their low concentration. Furthermore, diamagnetic minerals are high enough in concentration to effectively dilute and minimize the paramagnetic and ferrimagnetic minerals as indicated by weak to negative χ_{lf} values.

Fe-carbonate cemented samples (Fig. 5d; DDS-9, 12A, 20, and 26) primarily consist of paramagnetic and ferrimagnetic minerals as indicated by hysteresis loop shapes (Figs. 6c and d). Given that these samples are quartz arenites, diamagnetic mineral contributions are inferred. However, the diamagnetic signal is overshadowed by the magnetically stronger paramagnetic and ferrimagnetic minerals. Figure 5d shows that these samples are associated with anomalous peaks in κ values. Figure 11 indicates that these samples are associated with relatively low B_{CR} values (50.1 to 73.8 mT) and varying χ_{lf} values (0.5 to 10.8 $\times$ 10^{-8} m^3 kg^{-1}) relative to the quartz-cemented samples. Low B_{CR} values in DDS-9 and DDS-20 suggest that magnetite is the ferrimagnetic contributor, whereas higher B_{CR} values in DDS-12A and DDS-26 suggest that higher-coercivity ferrimagnetic minerals (e.g. SD magnetite/titanomagnetite or PSD titanomagnetite) may occur in the samples. The Day Plot (Fig. 12) indicates that magnetic grain-size of these samples primarily falls within the PSD region for magnetite. DDS-12A falls below the Dunlop and Ozdemir (1997) suggested PSD boundary ($B_{CR}/B_C \geq 2.0$), implying that a

bimodal grain-size distribution is occurring between SD and PSD grains. Therefore, the high-coercivity phase in DDS-12A is likely attributed to SD magnetite/titanomagnetite.

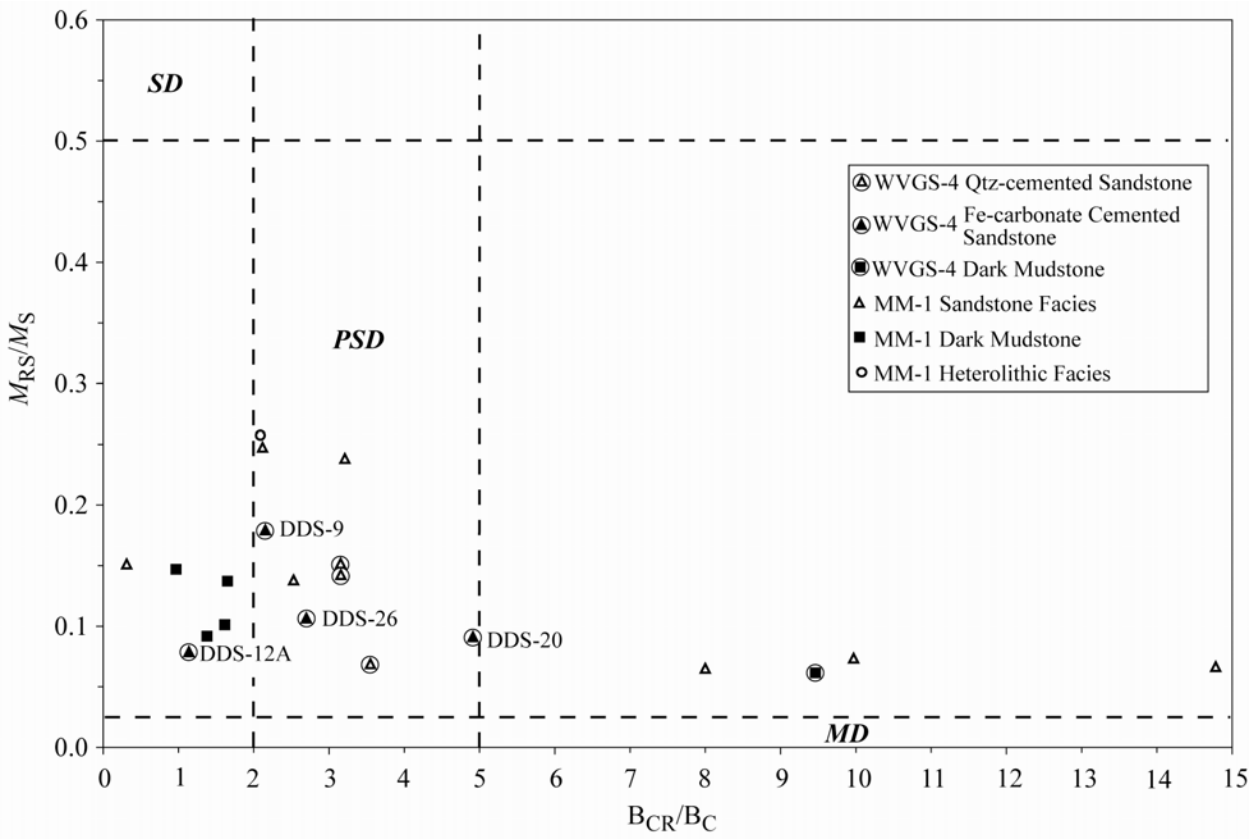

Figure 12 - Day Plot illustrating the effects of mineralogy and grain-size variations as a function of hysteresis ratios for lower Pennsylvanian samples. Single domain (SD), pseudo-single domain (PSD), and multidomain (MD) fields modeled after Dunlop and Ozdemir (1997) are shown.

Figure 13 shows that $\chi_h > \chi_{ferri}$ for the Fe-carbonate cemented sandstones, indicating that paramagnetic minerals are the dominant contributors to χ_{lf}. DDS-9 displays very low χ_h and χ_{ferri} values that can be explained by the low paramagnetic and ferrimagnetic concentration illustrated in Figure 14. Low magnetic concentrations in DDS-9 are likely responsible for the correlative lower susceptibility observed in the sample relative to the other Fe-carbonate cemented samples (Figs. 5d, 11, and 13). The paramagnetic mineral concentration is greater than the ferrimagnetic concentration for all of the Fe-carbonate cemented samples as illustrated in Figure 13. These relationships suggest that the magnetic susceptibility of the Fe-carbonate cemented samples is primarily controlled by paramagnetic minerals, and in particular their concentration.

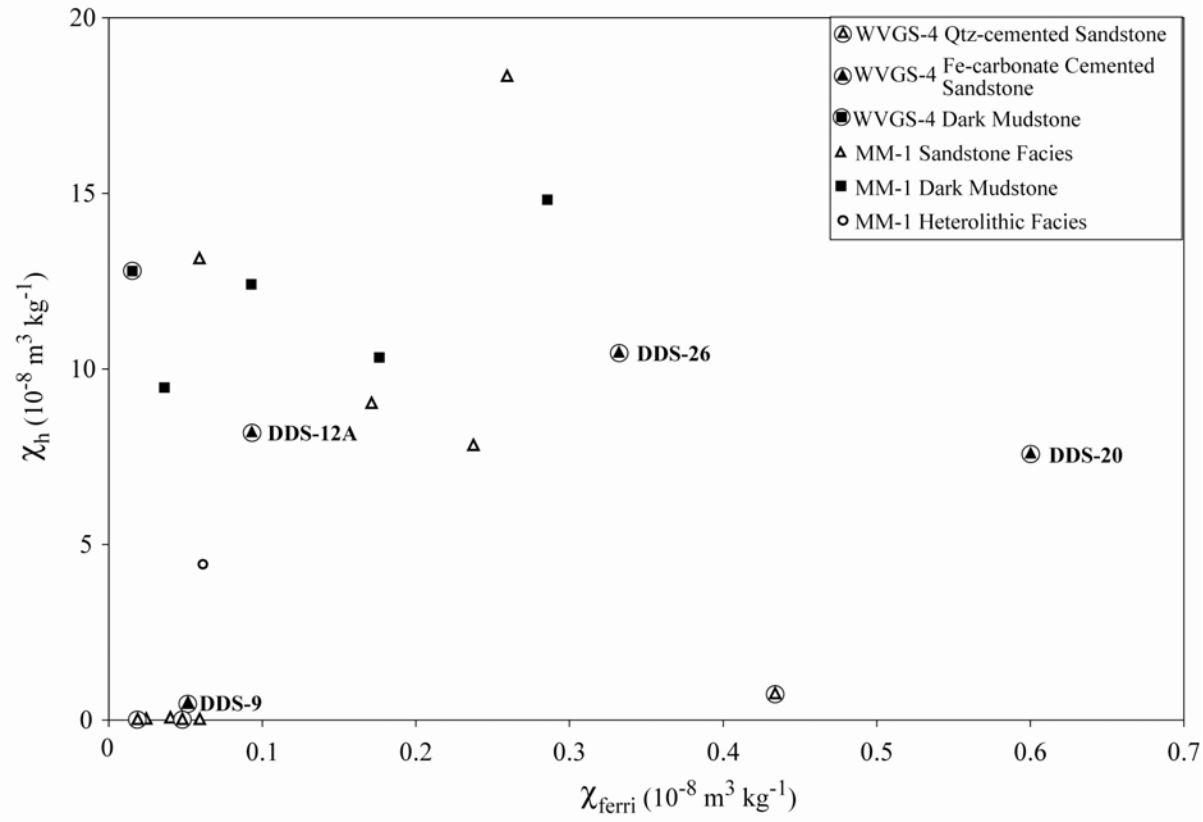

Figure 13 - Ferrimagnetic susceptibility (χ_{ferri}) vs. paramagnetic susceptibility (χ_h) for lower Pennsylvanian samples. χ_h = high-field (> 0.8 T) slope of hysteresis loop and is equivalent to the paramagnetic contribution to χ_{lf} since no antiferromagnetic minerals are present in these samples. $\chi_{ferri} = \chi_{lf} - \chi_h$ and is equivalent to the ferrimagnetic contribution to χ_{lf}.

MM-1 Samples

The MM-1 sandstone facies display similar κ trends compared to WVGS-4 sandstones (Figs. 5d and e) and are attributed to diamagnetic, paramagnetic and ferrimagnetic mineral phases as indicated by hysteresis loop shapes (Figs. 6c and g). Samples with low χ_{lf} values are largely associated with higher B_{CR} values (Fig. 11) and display strong diamagnetic and weak ferrimagnetic loop trends (e.g. Fig. 6c). In contrast, samples with higher χ_{lf} values have lower B_{CR} values and display strong paramagnetic and weak ferrimagnetic loop trends (e.g. Fig. 6c). Differences in B_{CR} and χ_{lf} values for these samples imply that a range of coercive phases are present (e.g. low-coercivity PSD and MD magnetite and higher-coercivity SD magnetite and/or titanomagnetite) suggesting that differences in mineral content, concentration, and grain-size occur between the samples. Antiferromagnetic loop characteristics (e.g. open loop above fields

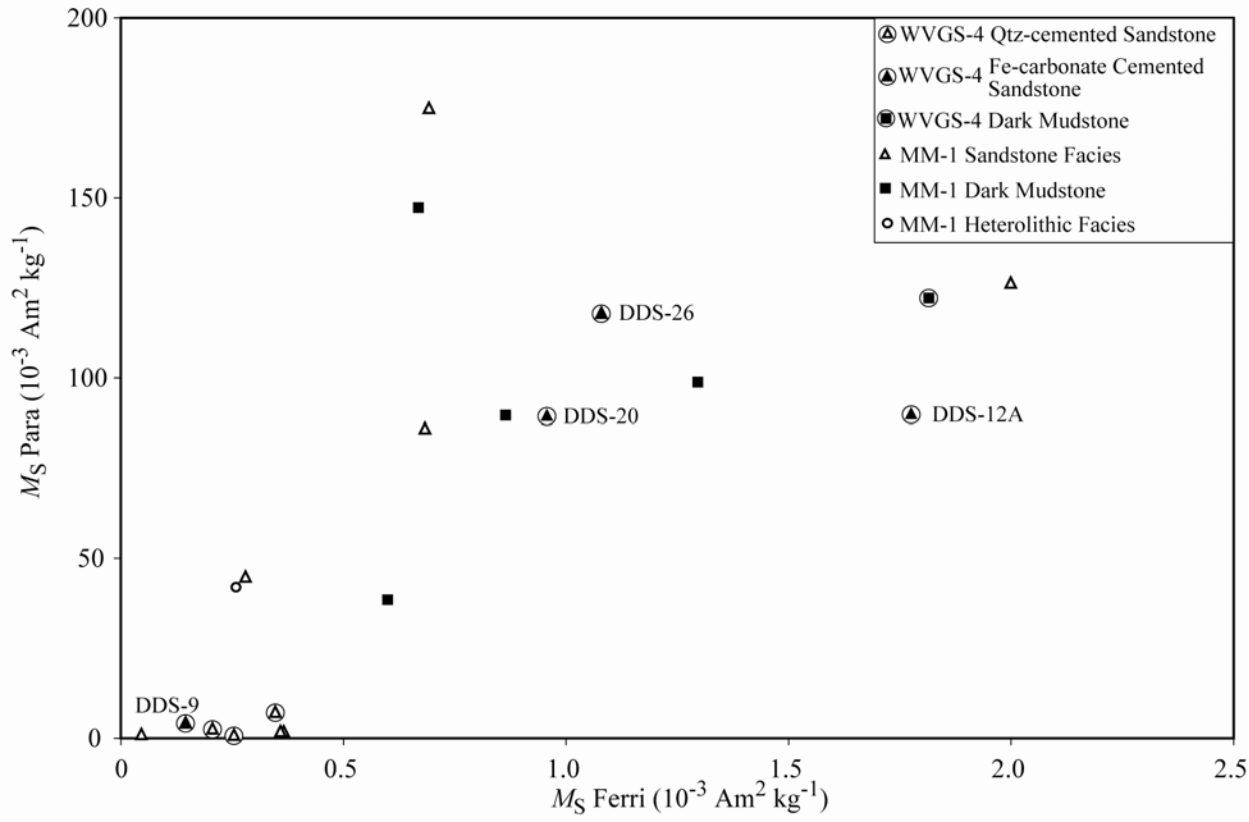

Figure 14 - Paramagnetic M_S vs. Ferrimagnetic M_S for lower Pennsylvanian samples. M_S is a concentration-dependent parameter that increases monotonically with the amount of magnetic material present. M_s Para refers to the paramagnetic M_S (e.g. Fe -carbonate cement and/or paramagnetic clay concentration) obtained from uncorrected hysteresis loops. M_S ferri reflects ferrimagnetic M_S (e.g. magnetite-titanomagnetite concentration) obtained from slope-corrected hysteresis loops, or antiferromagnetic M_S in samples lacking ferrimagnetic minerals (e.g. magnetite and titanomagnetite), or the combined antiferromagnetic M_S + ferrimagnetic M_S in samples associated with both ferrimagnetic and antiferromagnetic minerals (e.g. wasp-waisted hysteresis loops indicating magnetite and hematite).

of 0.4 T or wasp-waistedness) are not observed in any of the MM-1 quartz sandstone samples implying that high-coercivity antiferromagnetic minerals (e.g. hematite) are not responsible for elevated B_{CR} values. The Day Plot (Fig. 12) shows that three samples fall within the PSD boundary for magnetite suggested by Dunlop and Ozdemir (1997). However, three samples associated with higher B_{CR}/B_C values fall above the PSD boundary ($B_{CR}/B_C \geq 5.0$) and likely indicate that complex mixtures of magnetite grain-sizes are occurring between PSD and MD grains or that higher-coercivity mineral phases are present (e.g. SD magnetite or titanomagnetite). The sample with the highest B_{CR}/B_C value (14.8) is also associated with the

highest B_{CR} value (116.2 mT; Fig. 11) and suggests that titanomagnetite may be the ferrimagnetic mineral present. Two samples that fall below the PSD boundary ($B_{CR}/B_C \geq 2.0$) suggested by Dunlop and Ozdemir (1997) and are interpreted to reflect a bimodal grain-size distribution between SD and PSD magnetite grains within the sample.

Figure 13 shows that three MM-1 samples are associated with very low χ_h and χ_{ferri} values. These samples are also associated with diamagnetic loop characteristics and weak to negative χ_{lf} values. This indicates that diamagnetic minerals are effectively diluting the ferrimagnetic signal similar to that of the WVGS-4 quartz-cemented samples. Furthermore, concentration data (Fig. 14) show that these samples are also associated with very low paramagnetic and ferrimagnetic concentrations. This suggests that diamagnetic cements (e.g. quartz and calcite) are present in these samples. In comparison, the other MM-1 quartz-sandstone samples display high χ_h values and are associated with paramagnetic loop characteristics (e.g. Fig. 6c). M_S data also indicate that high concentrations of paramagnetic minerals occur in these samples (Fig. 14). High χh and paramagnetic M_S values imply that paramagnetic cements (e.g. siderite, ankerite, Fe-dolomite) are present in these samples in common with the WVGS-4 Fe-carbonate cemented samples.

Lithofacies G: Heterolithic Facies

The MM-1 tidal rhythmite sample is associated with a moderate κ value (Fig. 5e) and hysteresis loops indicate the presence of paramagnetic and ferrimagnetic minerals (Figs. 6c and d). This sample is associated with a low B_{CR} value (28.9 mT) indicative of the mineral magnetite, and a low χ_{lf} value (4.5×10^{-8} m^3 kg^{-1}; Fig. 10). The Day Plot (F ig. 12) indicates that the magnetic grain-size falls in the PSD region for magnetite.

χ_h (4.4×10^{-8} m^3 kg^{-1}) and χ_{ferri} (0.06×10^{-8} m^3 kg^{-1}) values indicate that paramagnetic minerals are the dominant contributors to χ_{lf} since $\chi_h > \chi_{ferri}$ (Fig. 13). The paramagnetic mineral concentration is greater than the ferrimagnetic concentration as illustrated in Figure 14. These relationships suggest that the magnetic susceptibility of these samples is primarily controlled by paramagnetic minerals (e.g. Fe-rich clays and cements), and in particular their concentration.

Lithofacies H: Dark Mudstone-Sandstone Facies

The WVGS-4 dark mudstone sample is associated with the highest observed κ value (Fig. 5d) attributed to paramagnetic and ferrimagnetic minerals as indicated by hysteresis loop shapes

(Figs. 6c and d). Figure 11 shows that the ferrimagnetic phase is related to higher-coercivity minerals (e.g. SD magnetite and titanomagnetite) since B_{CR} values are relatively high for this sample. Low M_{RS}/M_S and high B_{CR}/B_C values depicted on the Day Plot (Fig. 12) suggest that titanomagnetite (or mixtures of titanomagnetite and magnetite) may be responsible for the higher-coercivity phases and not mixtures of high-coercivity SD and low-coercivity PSD or MD magnetite. This interpretation is favored because mixtures of SD and coarser magnetite grains should produce lower B_{CR}/B_C and higher M_{RS}/M_S values as well as display notable wasp-waisted loop trends, none of which are observed in this sample.

χ_h and χ_{ferri} values indicate that paramagnetic minerals are the dominant contributors to χ_{lf} since $\chi_h > \chi_{ferri}$ (Fig. 13). Figure 14 indicates that the paramagnetic concentration is much greater that the ferrimagnetic concentration and suggest that the $\chi_h > \chi_{ferri}$ relationship is largely a function of the paramagnetic concentration. These relationships suggest that the magnetic susceptibility of these samples is primarily controlled by paramagnetic minerals (e.g. Fe-rich clays and/or cements), and in particular their concentration.

The MM-1 dark mudstone facies display moderate to high κ values (Fig. 5e). Hysteresis loops indicate that paramagnetic and ferrimagnetic minerals occur in the samples as indicated by hysteresis loop shapes (Figs. 6c and d). Figure 11 indicates that these samples are characterized by moderate χ_{lf} and low B_{CR} values. Low B_{CR} values and ferrimagnetic hysteresis loop characteristics suggest that magnetite is present. The Day Plot (Fig. 12) indicates that the magnetic grain-size of magnetite in these samples falls below the PSD boundary ($B_{CR}/B_C \geq 2.0$) implying that a bimodal grain-size distribution exists between SD and coarser magnetite grains within the sample.

χ_h and χ_{ferri} values indicate that paramagnetic minerals are the dominant contributors to χ_{lf} for the MM-1 dark mudstone facies since $\chi_h > \chi_{ferri}$ (Fig. 13). Figure 14 shows that the paramagnetic concentration is much greater that the ferrimagnetic concentration and imply that the $\chi_h > \chi_{ferri}$ relationship is largely a function of the paramagnetic concentration. These relationships suggest that the magnetic susceptibility of these samples is primarily controlled by paramagnetic minerals (e.g. Fe-rich clays and/or cements) and their concentration, in common with the WVGS-4 dark mudstone sample.

Correlation of χ_h and χ_{ferri} with M_S

Regardless of facies type, magnetic mineralogy, or grain-size, the Carboniferous samples analyzed in this study display a strong paramagnetic dependence on concentration. Figures 15a and b show that the paramagnetic susceptibility (χ_h) displays a strong positive correlation (R^2 = 0.99) with the paramagnetic concentration (M_S) for both upper Mississippian and lower

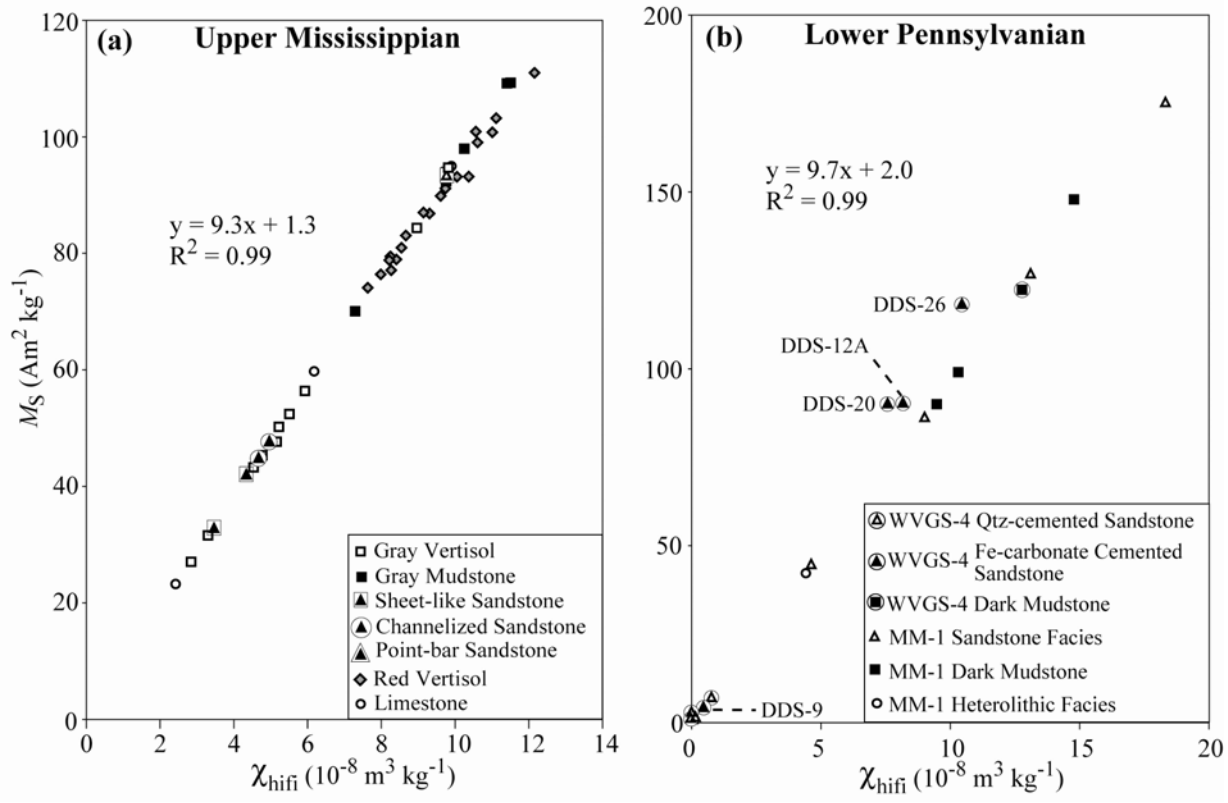

Figure 15 - χ_h vs Paramagnetic M_S for upper Mississippian (a) and lower Pennsylvanian (b) facies. High concentrations of paramagnetic and/or antiferromagnetic minerals plot high on these diagrams, whereas low concentrations of paramagnetic clays and antiferromagnetic minerals plot low. Strong linearity between χ_h and paramagnetic M_S suggests that χ_h is dominantly controlled by the concentration of paramagnetic materials.

Pennsylvanian samples. This suggests that the paramagnetic grain-size and mineralogy are subordinate to the concentration in terms of their influence on χ_h. With regard to facies types, the upper Mississippian facies show a separation between the sandstones, and gray vertisols and the gray mudstones and red vertisols, with some samples overlapping (Fig. 15 a). It appears that the red vertisols and gray mudstones are associated with the highest paramagnetic concentrations and consequently have higher χ_h values. Alternatively, the sandstones and gray vertisols are

associated with lower paramagnetic concentrations and consequently lower χ_h values. The limestone samples overlap both the high and low paramagnetic M_S and χ_h samples. In contrast to the paramagnetic M_S vs. χ_h, the ferrimagnetic concentration vs. χ_{ferri} (not shown) are very poorly correlated (< <1%), suggesting that the magnetic mineralogy, and grain-size may have a greater influence on χ_{ferri}.

Temperature Dependent Magnetic Results

TDS data (Figs. 16a and b) shows mineral magnetic phase transitions that are likely associated with iron-sulfide minerals (e.g. pyrrhotite or greigite) converting to magnetite in the upper section of the PWV-1 gray vertisol (Fig. 5b; 6.7m). The heating curve (Figs. 16a and b) is flat from room temperature to 260^{o}C, suggesting that greigite is not present since there is no susceptibility loss due to its decomposition at ~200^{o}C (e.g. Torii et al., 1996). The increase at 260^{o}C could correspond to the λ-transition of pyrrhotite from antiferromagnetic to ferrimagnetic phase (Rochette et al., 1990; c.f. Kontny et al., 2000.) However, antiferromagnetic loop trends (e.g. open loops above ~ 0.4 T; Fig. 6a) are not observed on initial room temperature loops. At 315^{o}C, susceptibility drops, possibly indicating that ferrimagnetic pyrrhotite (T_C = 320^{o}C) was formed. At 530^{o}C another susceptibility peak arises, possibly due to the conversion of some iron sulfide phase to magnetite and/or the transformation from iron-bearing silicates and clays to magnetite (Zhu et al., 2001). The newly formed mineral phase is magnetite, as suggested by its drop in κ at 580^{o}C. The cooling curve (Fig. 16a) displays a sharp susceptibility rise at 580^{o}C, due to the formation of magnetite upon heating, and peaks at 455^{o}C. Susceptibility continues to decrease until 230^{o}C where it sharply increases and peaks at 165^{o}C. The peak at 165^{o}C suggests that some other remanence carrying mineral phases were formed during initial heating. However, their identity cannot be discerned by the TDS data. Susceptibility decreases with continued cooling from 165^{o}C back to room-temperature. Overall, the TDS data indicate that greigite is not likely present in the sample. However, due to the complexity of the heating-cooling TDS curve, the conversion of some iron sulfide phase to magnetite and/or the transformation from iron-bearing silicates and clays to magnetite are the best interpretation of the TDS patterns observed in the gray vertisol sample. Although not conducted here, step-wise heating and cooling TDS experiments (e.g. Hrouda et al., 2003; Liu et al., 2005) may provide additional insight into the mineral phase transitions observed in the TDS data for this sample.

Figure 16

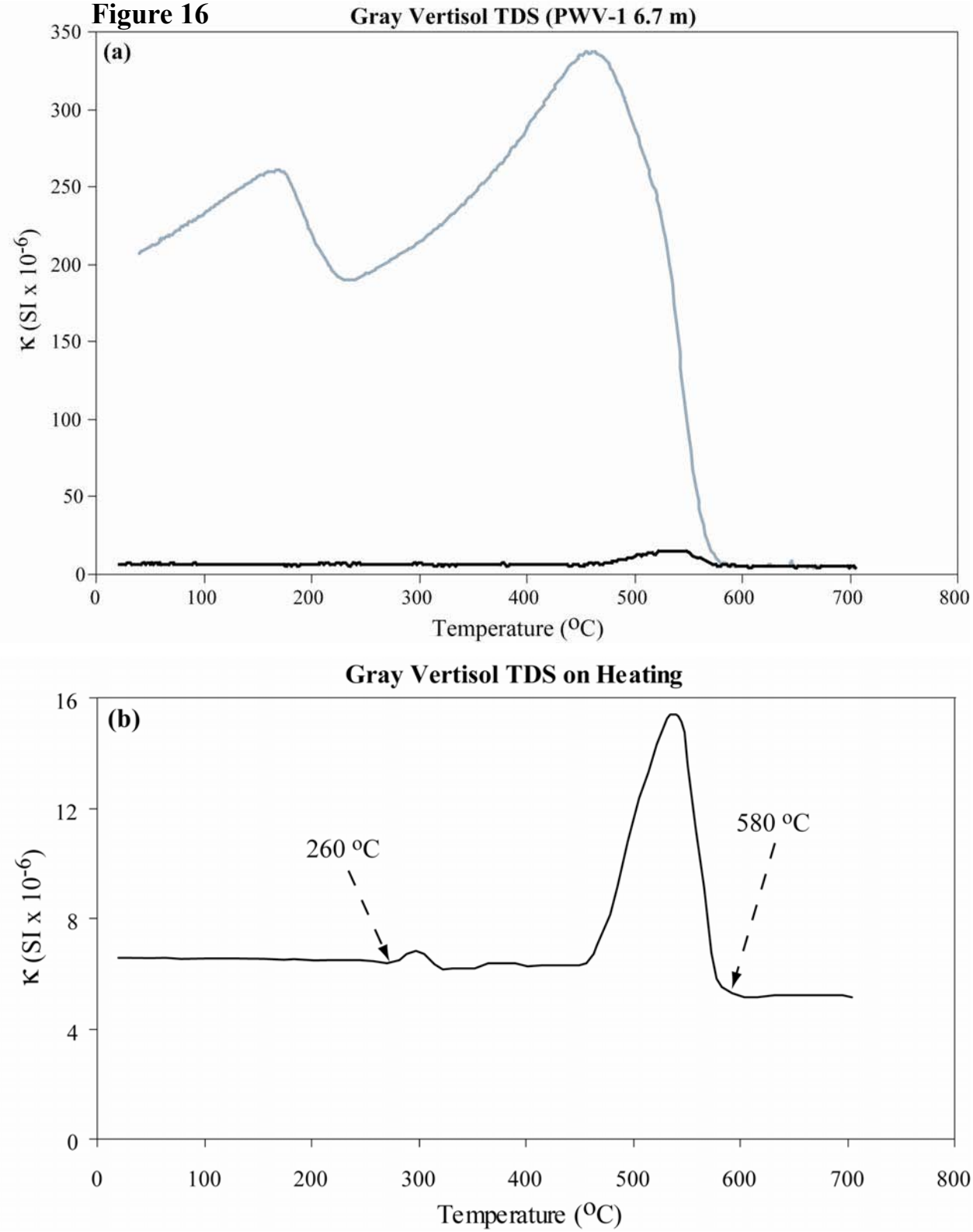
Gray Vertisol TDS (PWV-1 6.7 m)
(a)
κ (SI x 10-6)
Temperature (°C)
Gray Vertisol TDS on Heating
(b)
260 °C
580 °C
κ (SI x 10-6)
Temperature (°C)

Figure 16 - Temperature-dependent susceptibility (TDS) for upper Mississippian PWV-1 gray vertisol sample showing iron sulfide/Fe-clay transformation to magnetite. (a) Heating curve showing the formation of a new ferrimagnetic mineral phase with a peak at 530°C. The loss of susceptibility at 580°C indicates that the newly formed mineral phase is magnetite. Cooling curve shows characteristic magnetite increase at 580°C; however with continued cooling another susceptibility peak appears at 165°C implying that complex unidentified ferrimagnetic iron sulfide phases were formed during heating. (b) Enhanced heating-curve from above illustration indicates that a new iron sulfide mineral phase was formed at 260°C with a Curie temperature of ~320°C similar to pyrrhotite.

Figure 17 shows the temperature dependent ferrimagnetic component of magnetization as a percentage of the total temperature dependent M_S for three different cement types (siderite, ankerite, and Fe-dolomite) within the lower Pennsylvanian WVGS-4 quartz arenite facies. Below 300°C all three cement types have a similar low percentage of ferrimagnetic minerals. Between 300 and 400°C slight increases in ferrimagnetic minerals are observed in the three samples with siderite having the greatest percent gain. Between 400 and 500°C the siderite-cemented sample shows a marked increase in the percent of ferrimagnetic minerals in the sample. This occurrence is consistent with a siderite to magnetite transformation obtained by TDS measurements in other studies (e.g. Ellwood et al., 1989; Pan et al., 2000). The ankerite and Fe-dolomite samples also suggest that a mineral phase transition is occurring between 400 and 500°C. However, the amount of ferrimagnetic minerals transformed from these two cement types is much less than that of siderite. This is likely due to ankerite and Fe-dolomite transforming into some spinel structure similar to magnetite (e.g. maghemite) with less Fe in the crystal lattice. TDS data (Figs. 18a, b, and c) also show the mineral magnetic phase transitions for siderite and ankerite cements. Upon heating the siderite-cemented sample, κ decreases before reaching 250°C (Fig. 18a inset), indicating the dominant contribution of paramagnetic siderite (Pan et al., 2000). After ~ 365°C, however, κ increases sharply indicating the generation of a new ferrimagnetic mineral phase. The drop in κ between 540 – 590°C indicates that the Curie point of magnetite has been reached (T_C = ~ 580°C) and ferrimagnetism is lost. Upon cooling, the susceptibility remains low until ~ 580°C where a sharp increase in κ occurs forming a peak also characteristic of magnetite. Susceptibilities on heating the ankerite sample decrease before reaching 200°C, and likely indicate the dominant contribution of paramagnetic ankerite (Fig. 18b). Continued heating shows an increase in κ from ~ 410 to 500°C indicating that a new ferrimagnetic phase has been generated (Fig. 18 b).

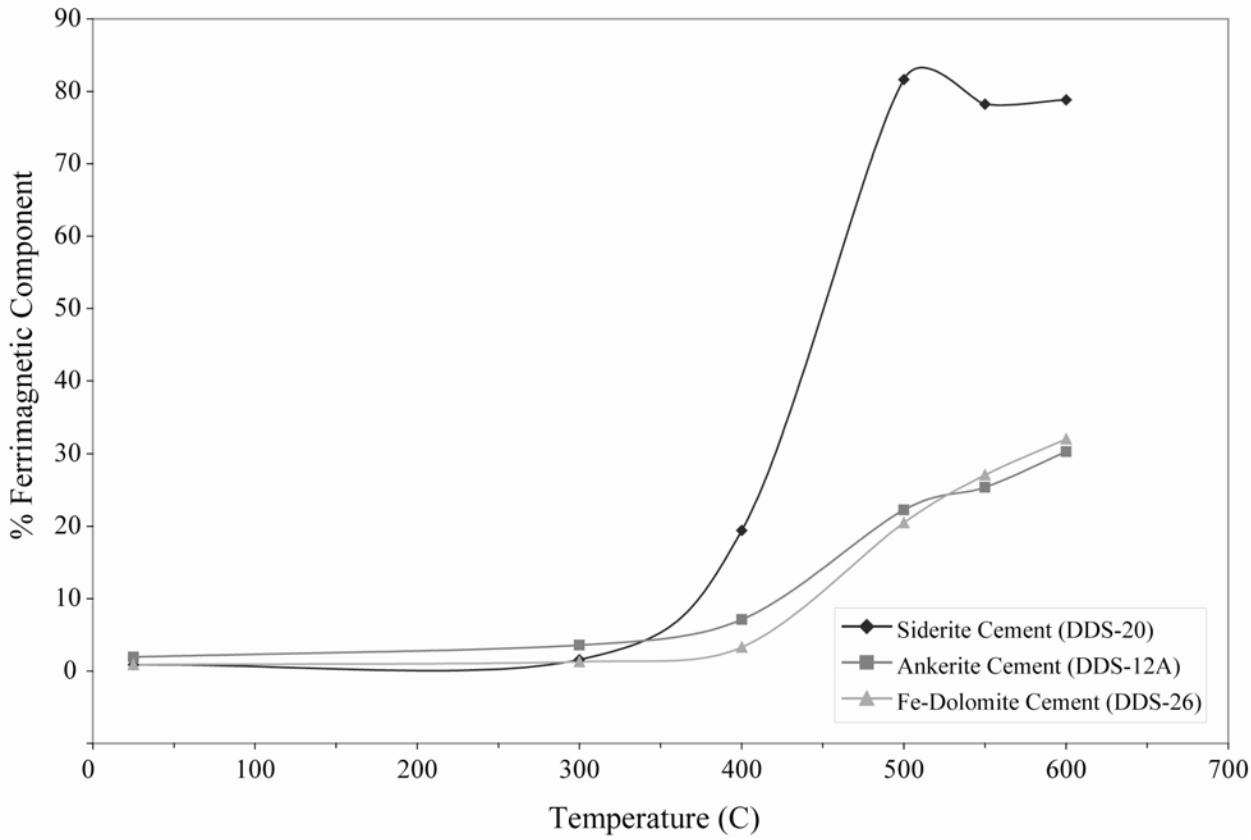

Figure 17 - Stepwise thermal hysteresis acquisitions showing the percent of ferrimagnetic components in three lower Pennsylvanian Fe-carbonate cemented samples (DDS-12A, DDS-20, and DDS-26) after each heating step. Increases in slope indicate that new ferrimagnetic phases are being formed. The amounts of ferrimagnetic minerals transformed from siderite are much greater than for ankerite and Fe-dolomite. This is reflective of iron availability within the initial carbonate crystal lattices. Since siderite has a greater amount of Fe in its lattice, more magnetite can be formed by oxidation as the sample is heated.

The drop in κ between ~ 500 and 590^{o}C indicates the Curie temperature for magnetite where ferrimagnetism is lost. Upon cooling, the susceptibility slowly begins to rise at 580^{o}C; however at ~ 540^{o}C a dramatic increase in susceptibility occurs as cooling continues (Fig. 18c). The slight increase at 580^{o}C followed by the dramatic increase at 540^{o}C suggests that some ankerite converted to magnetite upon heating. However, the dramatic increase at ~ 540^{o}C suggests that the majority of minerals transformed from the ankerite cement did not form magnetite but instead likely oxidized to form some spinel structure with iron incorporated into the crystalline lattice. The differences in peak κ values (both heating and cooling) between the siderite and

Figure 18

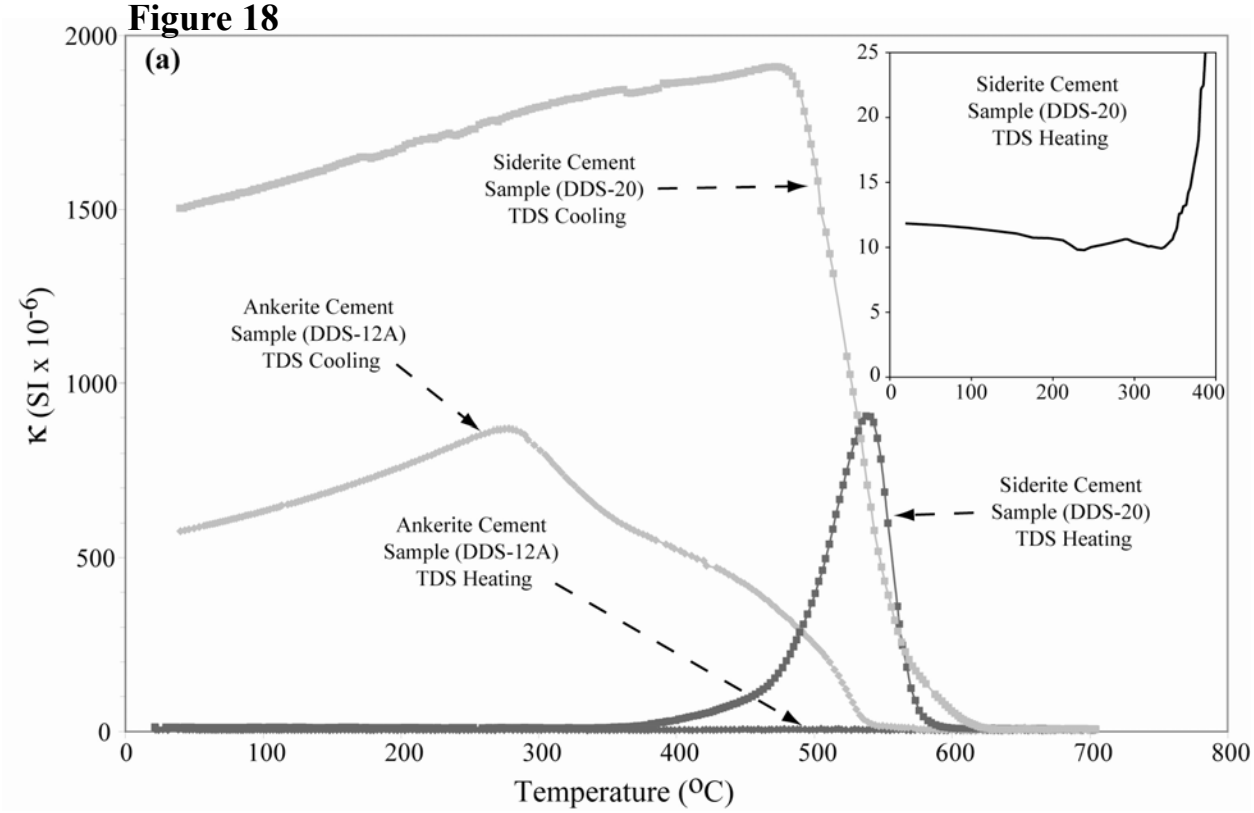
(a)
Siderite Cement Sample (DDS-20) TDS Cooling
Ankerite Cement Sample (DDS-12A) TDS Cooling
Ankerite Cement Sample (DDS-12A) TDS Heating
Siderite Cement Sample (DDS-20) TDS Heating
Siderite Cement Sample (DDS-20) TDS Heating
κ (SI x 10-6)
Temperature (°C)

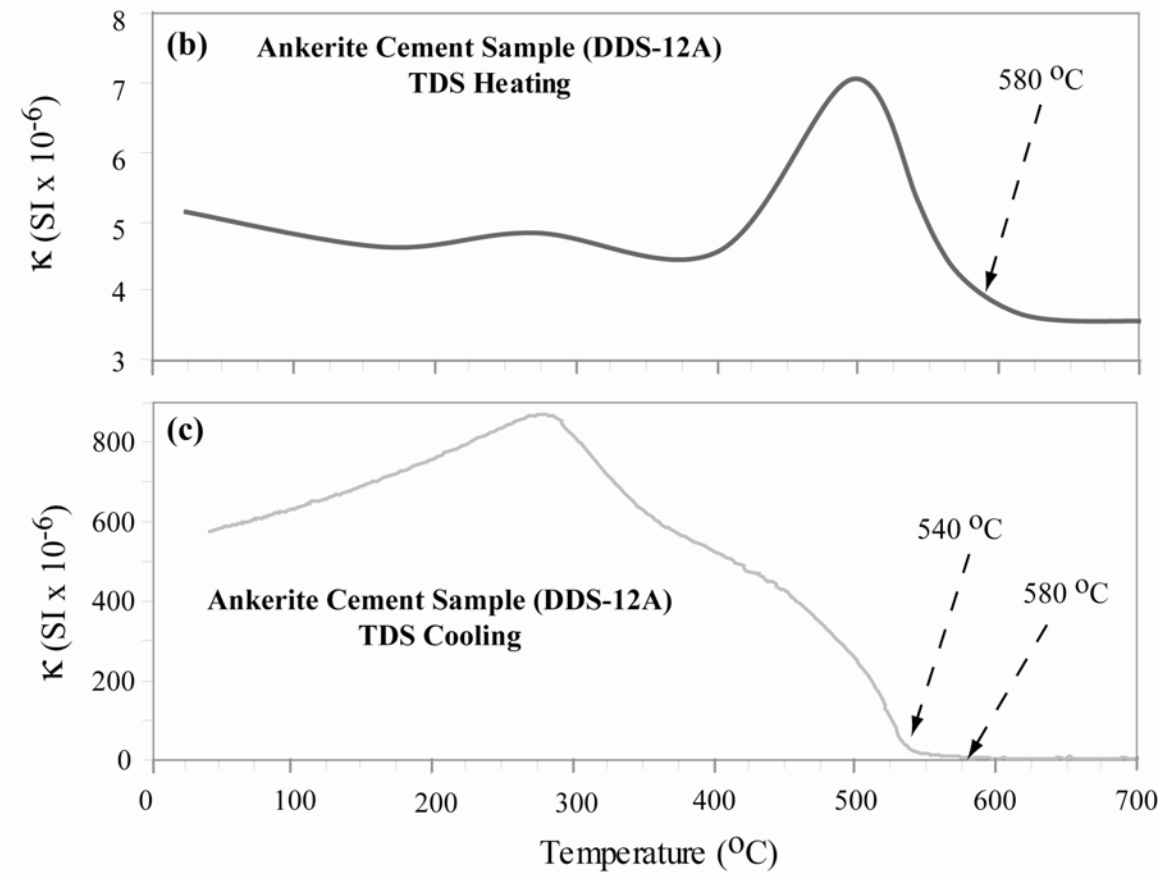
(b)
Ankerite Cement Sample (DDS-12A) TDS Heating
580 °C
(c)
Ankerite Cement Sample (DDS-12A) TDS Cooling
540 °C
580 °C
κ (SI x 10-6)
Temperature (°C)

Figure 18 - Temperature-dependent susceptibility (TDS) curves for lower Pennsylvanian siderite (DDS-20) and ankerite (DDS-12A) cemented quartz arenite samples. (a) Heating-cooling curve indicates that the siderite sample produces a greater amount of strong ferrimagnetic minerals on heating compared to ankerite. Inset shows the decay in susceptibility on heating to ~250^{o}C indicating that the sample was dominantly paramagnetic. (b) Ankerite heating curve showing similar decay in susceptibility to ~190^{o}C and the generation of new ferrimagnetic phases at ~500^{o}C. (c) Ankerite cooling curve showing slight increase in susceptibility at 580^{o}C attributed to low concentrations of magnetite formed by heating, and a sharp susceptibility increase at 540^{o}C indicating that a high concentration of an unidentified ferrimagnetic phase resulted from heating.

ankerite cement is attributed to Fe availability. Siderite has more Fe available in the crystal lattice to transform; therefore it produces more magnetite and higher susceptibilities.

Interpretation of Magnetic Facies

Mineral magnetic results from Carboniferous fluvial/alluvial strata in the Central Appalachian Basin are interpreted to reflect variations in parent material, pedogenic alteration, and/or diagenetic modification of the original magnetic signal.

Upper Mississippian Magnetic Signals

Primary depositional signals as well as pedogenic and early diagenetic signals are preserved in the upper Mississippian samples including: (1) detrital magnetite-titanomagnetite in channelized and point-bar sandstones and gray mudstones, and detrital magnetite-titanomagnetite and hematite in sheet-like sandstones and limestones; (2) early diagenetic signals in sheet-like sandstones; and (3) pedogenic signals in red and gray vertisols.

Depositional Signals

Detrital Magnetite-titanomagnetite

Magnetite-titanomagnetite identified in the channelized and point-bar sandstones, as well as in the gray mudstone and limestone facies is, on the basis of hysteresis behavior (e.g. Figs. 6c and d; Figs. 7 and 8), interpreted as detrital rather than authigenic. The most plausible non-pedogenic, post-depositional modes of magnetite formation documented in the literature include the dehydration of goethite to hematite (Ozdemir and Dunlop, 2000; and references therein), and the oxidation of siderite to hematite (Ellwood et al., 1986, 1988, 1989; Pan et al., 2000).

Magnetite is produced as an intermediate phase in these reactions. However, source area provenance is the most likely explanation for the occurrence of magnetite in these samples because it occurs in channel sandstones as well as in clay-rich sediments deposited by overbank flooding of river channels. Similarity in ferrimagnetic mineralogy, concentration, and grain-size between the channelized sandstone and gray mudstone (Figs. 7, 8, 9, and 10) suggests that the magnetite-titanomagnetite was not produced authigenically because it seems unlikely that nearly identical mineralogies, concentrations, and grain-sizes would be produced by the authigenic alteration of goethite or siderite to magnetite in two mineralogically and granulometrically different facies (lithic sandstone vs. gray mudstone).

Most workers have attributed Appalachian Basin Carboniferous sandstone compositions to recycling of detritus from the Appalachian orogenic province to the southeast of the depositional basin (Houseknecht, 1980; Dickinson et al., 1983; Donaldson et al., 1985; McDowell, 1986; Reed at al., 2005). Magnetite/titanomagnetite was likely derived from the orogenic province and incorporated into incised valley trunk-tributary drainage networks represented by the channelized, point-bar and sheet-like sandstones and associated grey mudstones of floodplain origin (Miller and Eriksson, 2000).

Detrital Hematite

Most of the hematite in the sheet-like sandstones, identified on the basis of hysteresis characteristics and high B_{CR} values (e.g. Figs. 6a and b; Fig. 7)**,** is also interpreted as detrital. Red mudstone and siltstone intraclasts are the likely source of the detrital high-coercivity (hematite) mineral phases in these sandstones. These intraclasts were derived locally in response to sheet flooding across oxidized floodplain sediments.

Detrital Magnetite-titanomagnetite and Hematite

Magnetic characteristics of the limestone facies, reveal a two-component magnetic system between mixtures of magnetite/titanomagnetite and hematite in two samples, as indicated by wasp-waistedness (e.g. Figs. 6a and b), and exclusively titanomagnetite in another, as indicated by a lower B_{CR} value (Fig. 7). A detrital origin for these magnetic constituents is based on the same criteria used above. Changes in sediment influx are the simplest explanation for the mineralogic and concentration differences (Figs. 7 and 10) observed in these samples. Wetter

times would likely have promoted increased discharge into the playa. As a result, increased overland runoff that incorporated red sediments from surrounding red upland soils would have carried hematite-rich silts and clays into the playa. Therefore, magnetite/titanomagnetite influx from source streams likely mixed with the hematite-rich sediments. These limestone samples lack red coloration and do not display SP hysteresis behavior (e.g. closed loops at all fields) suggesting that hematite was not formed *in situ* by the dehydration of goethite. Furthermore, hematite formed by the *in situ* oxidation of magnetite/titanomagnetite would require that the lake sediments were subaerially exposed. This would likely result in the formation of a calcic protosol (sensu Mack et al., 1993) and/or development of red pigmentation, neither of which are observed in these samples.

Early Diagenetic Signals

Another source of hematite in the sheet-like sandstones is through the oxidation of detrital magnetite/titanomagnetite, and possibly the conversion of some ferromagnesian clays (e.g. illite, smectite, and chlorite), as the sediment dewatered on an exposed floodplain. Given the nature of these sandy crevasse splay deposits, it seems logical that both the incorporation of hematitic siltstone/mudstone interclasts and the oxidation of primary magnetite/titanomagnetite are responsible for the high-coercivity antiferromagnetic mineral (hematite) phases (e.g. Figs. 6a and b; Fig. 7). This indicates that the sources of hematite include both primary depositional (red mudstone and siltstone interclasts) and post depositional (the oxidation of magnetite/titanomagnetite and possibly the alteration of ferromagnesian clays) processes.

Pedogenic Signals

Red Vertisols

Red vertisols display κ profiles that reflect magnetic enrichment, depletion, and vertical amalgamation. Magnetic enrichment is demarcated by high κ values within many of the red vertisols (Fig. 5c). Enrichment in κ coincides with high χ_h and paramagnetic M_S (Fig. 15a) suggesting that the magnetic susceptibility patterns are related to illuvial increases in paramagnetic clays such as smectites and illites.

Magnetic depletion in κ profiles occurs in the upper and lower parts of some red vertisol profiles (Fig. 5c). Depletion in κ in the upper parts of soil profiles coincides with lower χ_h and

paramagnetic M_S values (Fig. 15a), suggesting that elluviation of paramagnetic clays occurred in the upper B horizons. The wasp-waisted trends in the upper elluvially depleted horizons (e.g. Fig. 6b) indicate the presence of mixed magnetite and hematite. Magnetic depletion in the lower parts of soil profiles (Fig. 5b and c) is also associated with decreases in paramagnetic concentrations. However, elluviation is not the likely cause. Instead, decreases in magnetite coincide with increases in hematite as indicated by the decrease and eventual disappearance of ferrimagnetic phases in wasp-waisted loops (e.g. the loop in Fig. 6b becomes the loop in Fig. 6f). Downward increases in hematite at the expense of magnetite can be explained by long sustained periods of oxidation of magnetite to hematite. Magnetite was completely oxidized to hematite in the lower, older parts of the soil profile resulting in the lower magnetic susceptibility values. Vertical magnetic amalgamation is recorded by alternating low and high κ values in middle parts of thick vertisol profiles (Fig. 5c). Amalgamation is attributed to vertic shear mechanisms that effectively mixed the magnetic minerals.

Hematite in the red vertisol facies was likely formed by the oxidation of primary magnetite-titanomagnetite and Fe-bearing silicates prior to burial, and not from the dehydration of goethite or oxidation of siderite. The dehydration of goethite generally produces crystals < 0.03 μm in size (Dunlop and Ozdemir, 1997), making them superparamagnetic (SP) and will not acquire remanence. Hematite identified in all of the upper Mississippian facies caries a strong remanence magnetization (e.g. Fig. 6b and f). Therefore, magnetite-titanomagnetite and possibly Fe-bearing silicates present in original flood-plain sediments was partially oxidized shortly after deposition. If hematite formed by the near-surface oxidation of diagenetic siderite following exhumation, then the gray mudstone facies would be expected to contain and to have acquired red pigmentation as is the case for the red vertisols.

Gray Vertisols:

In gray vertisols thick enough to show discernable trends, κ profiles show evidence of magnetic depletion and enrichment (Figs. 5a and b). The most obvious zone of magnetic enrichment occurs in the ~7.5 m thick PWV-1 stacked, gray vertisol profile that displays an increase in κ over the 9 to 10 m interval (Fig. 5b). This enrichment coincides with increases in χ_{ferri} (Fig. 9; 2 to 19 × 10^{-8} m^3 kg^{-1}), ferrimagnetic M_S (Fig. 10; 0.8 to 1.7 × 10^{-3} Am^2 kg^{-1}), and in paramagnetic parameters M_S (Fig. 10; 50 to 84 × 10^{-3} Am^2 kg^{-1}) and χ_h (Fig. 9; 5 to 9 × 10^{-8} m^3

kg^{-1}). Increases in the paramagnetic parameters imply that paramagnetic clays were transported and concentrated by illuviation whereas increases in the ferrimagnetic parameters suggest that iron became reduced, mobilized, transported downward in the soil profile and subsequently re-oxidized as magnetite/titanomagnetite. The presence of magnetite/titanomagnetite is inferred due to the ferrimagnetic loop trends (Fig. 6c and d) and low B_{CR} values (Fig. 7). Magnetic depletion due to removal and translocation of iron species at the 9m depth interval for the PWV-1 gray vertisol (Fig. 5b) is likely responsible for the lower κ values observed in this part of the profile. Mobilization of Fe most likely occurred during wetter times when an elevated water-table promoted Fe^{+3} reduction. A subsequent drop in the water-table would have lowered the reduction front and allowed the mobilized iron to re-oxidize and precipitate.

The upper section of this gray vertisol (Fig. 5b, 6.7 to 7.4 m) displays similar patterns of depletion and enrichment. However, temperature dependent susceptibility data (Figs. 17a and b) indicate that iron sulfide minerals (e.g. pyrrhotite) may be responsible for the ferrimagnetic hysteresis components observed in the hysteresis data (Figs. 7, 9, and 10). The origin of iron sulfides may be a result of active reduction of magnetite in an organic-rich anaerobic soil or may be later during diagenetic sulfate reduction. The location of these samples below a coal suggests that primary, detrital magnetite-titanomagnetite may have been reduced as the soil became water-logged. Associated organic and sulfuric acids derived from the overlying coal may have reduced Fe^{+3} phases to complex and form iron sulfide phases. In diagenetic environments involving sulfate reduction, dissolved ferrous ions react with H_2S to form iron sulfide phases (Liu et al., 2004). Therefore, in addition to early iron reduction from organic acids, later diagenetic modes of sulfide formation (e.g. sulfate reduction) cannot be disregarded.

The above observations imply that the preserved magnetic character of the red and gray vertisols primarily reflects Mississippian pedogenic signals related to magnetic enrichment, depletion, and amalgamation. Undoubtedly, factors controlling the preserved pedogenic and diagenetic signals are complex and require careful consideration of environmental factors responsible for oxidation and reduction of magnetic particles, such as climatic variability, detrital mineralogy, available organic matter, post-depositional alteration of clays and primary detritus, pore fluid chemistry, and the duration and intensity of oxidation.

Lower Pennsylvanian Magnetic Signals: Core WVGS-4

Early and late diagenetic signals are preserved in lower Pennsylvanian sandstones from core WVGS-4 including: (1) an early diagenetic magnetite-titanomagnetite signal in the quartz-cemented sandstones (Fig. 5d); (2) early diagenetic paramagnetic signal in siderite cemented sandstones (Fig. 5d); and (3) near surface oxidation of deep burial ankerite and Fe-dolomite cements (Fig. 5d). In addition, the dark mudstone sample (Fig. 5d) is associated with high concentrations of paramagnetic minerals thought to reflect contributions from Fe-rich clays and diagenetic Fe-carbonate cements.

Early Diagenetic Magnetite-titanomagnetite

Reed et al. (2005) demonstrated petrographically that iron oxides developed as thin coatings on primary grains early in the diagenetic history of quartz-cemented sandstones implying communication with an oxygenated atmosphere. Subsequent deeper burial resulted in late-stage cements that are typically quartz and occur as syntaxial overgrowths and/or prismatic crystals that protrude into secondary pores. Magnetic analysis shows that these samples are dominated by weak (often negative) κ and χ_{lf} values (Figs. 5d and Fig. 11) that are characteristic of diamagnetic mineral assemblages with little ferrimagnetic or paramagnetic influence. Hysteresis data suggests that the iron oxide coatings are magnetite/titanomagnetite identified on the basis of low saturation fields (< 0.3 T, e.g. Fig. 6d) and low B_{CR} values (Fig. 11). Furthermore, low χ_{ferri} and ferrimagnetic M_S (Figs. 13 and 14) values indicate that magnetite/titanomagnetite occurs in a very limited quantity as suggested by the weak and negative κ and χ_{lf} values. The addition of late-stage diagenetic quartz cements may have lowered the initial magnetite/titanomagnetite signal by volume dilution (e.g. Soregan et al., 2002).

Early Diagenetic Siderite

As previously discussed, Reed et al. (2005) have shown that wheat-seed and euhedral siderite cements developed as primary pore filling cements early in the diagenetic history of the sandstones and reflect reducing pore-fluid conditions. Profiles of κ (Fig. 5e) show that the siderite-cemented sandstones (DDS-9 and DDS-20) are magnetically enhanced relative to the quartz-cemented sandstones. Hysteresis results (Fig. 13 and 14) indicate that this enhancement is largely attributed to increased paramagnetic influence (e.g. siderite cement) on the basis of $\chi_h >>$

χ_{ferri} and elevated paramagnetic M_S values. Microprobe results from Reed et al. (2005) confirm that siderite is the paramagnetic mineral phase present these samples, as also suggested by temperature-dependent hysteresis and TDS data (Figs. 17 and 18a).

Depleted $\delta^{18}O$ values (-12 to -13‰ PDB) from siderite rims indicate a meteoric water influence and support petrographic evidence that siderite formed relatively early (Reed et al., 2005). Furthermore, Mozely (1989) indicates that since sulfate activity is low in meteoric water, pyrite precipitation is inhibited resulting in more Fe^{+2} available for siderite formation. Postma (1982) lists two proposed mechanisms for siderite formation: (1) the replacement of $CaCO_3$; and (2) the reduction of ferric oxides by organic matter. The replacement of $CaCO_3$ is unlikely in the siderite cemented samples since Reed et al. (2005) indicate that these cements formed from meteoric pore fluids. In addition, these authors suggest that the main source of Fe^{+3} was transported in by terrestrial soils and streams and likely reduced to form siderite by Fe-reducing microbes under ever-wet climatic conditions.

Late Diagenetic Ankerite and Fe-Dolomite

Petrographic observations show that ankerite and Fe-dolomite formed during deep burial and after formation of secondary porosity (Reed et al., 2005). These authors also point out that later oxidation of the deep burial Fe-carbonate cements occurred in near-surface environments following exhumation. κ profiles (Fig. 5d) indicate that the ankerite sample (DDS-12A) and the Fe-dolomite sample (DDS-26) display elevated values similar to those of the siderite samples (DDS-9 and DDS-20). Temperature-dependent hysteresis and TDS data (Figs. 17 and 18a, b, and c), together with microprobe analysis (Reed et al., 2005), confirm that ankerite and Fe-dolomite are the paramagnetic minerals largely responsible for the magnetic susceptibility enhancement in DDS-12A and DDS-26. Room-temperature hysteresis characteristics (saturation field < 0.3 T and moderate B_{CR} and ferrimagnetic M_S values) reveal that magnetite and/or titanomagnetite is present in DDS-12A and DDS-26 (e.g. Figs. 6h; Figs. 11, and 14). Therefore, the Fe-oxides identified in DDS-12A and DDS-26 by Reed et al. (2005) are likely magnetite and/or titanomanetite. Based on the diagenetic interpretation of Reed et al. (2005), the ankerite and Fe-dolomite cemented samples are considered to reflect a near-surface ferrimagnetic signal where magnetite/titanomagnetite formed by partial oxidation of late burial Fe-carbonate cements following exhumation. This signal is superimposed on a paramagnetic deep-burial signal where

late ankerite and Fe-dolomite cements formed by the introduction of Fe-rich fluids. Magnetite/titanomagnetite identified in the early siderite samples (DDS-9 and DDS-20) on the basis of ferrimagnetic loop shapes and low to moderate B_{CR} values (Figs. 6h and 11) may also have formed by near-surface oxidation of Fe-carbonate cements following exhumation similar to DDS-12A and DDS-26.

Thin-section analysis of the WVGS-4 dark mudstone sample reveals that it is dominated by depositional clay minerals with lesser amounts of Fe-carbonate, quartz and Fe-oxide cements. The high κ value (Fig. 5d) is largely attributed to high concentrations of paramagnetic clays and Fe-carbonate cements. Hysteresis data confirm that increased paramagnetic contributions are responsible for the susceptibility enhancement on the basis of high χ_h and paramagnetic M_S and low χ_{ferri} values (Figs. 13 and 14). Low concentrations of magnetite/titanomagnetite have also been identified in these samples by low ferrimagnetic saturation (< 0.3 T) characteristics, low B_{CR}, and low ferrimagnetic M_S values (e.g. Fig. 6h; Figs. 11, and 14).

Lower Pennsylvanian Magnetic Signals: Core MM-1

Diagenetic inferences can be made for core MM-1 by comparing the combined diagenetic and magnetic interpretations of core WVGS-4 with the magnetic results from MM-1. Three MM-1 quartz arenite samples display weak negative κ values (27.3, 45.7, and 63.6 m, Fig. 5e) characteristic of quartz-dominated sandstones. These samples are associated with strong diamagnetic signals attributed to detrital quartz grains and diagnetic cements. This is suggested by weak negative χ_{lf} values, negligible χ_h and χ_{ferri} values, and low paramagnetic and ferrimagnetic M_S values, all of which are characteristic of the WVGS-4 quartz-cemented sandstones (Figs. 11, 13, and 14). Magnetite/titanomagnetite identified on the basis of hysteresis loop shape and low to moderate B_{CR} values (Figs. 6h and 11) in these quartz-dominated MM-1 sandstone samples are likely of similar origin to the early Fe-oxide coats identified by Reed at al. (2005) in WVGS-4. The magnetic characteristics of the MM-1 samples (27.3, 45.7, and 63.6 m, Fig. 5e) largely agree with those of the WVGS-4 quartz-cemented sandstones. Consequently, it seems reasonable to assume that a similar diagenetic history existed in the three MM-1 quartz dominated samples. Therefore, low concentrations of magnetite/titanomagnetite identified in these MM-1 sandstone samples likely developed as early coats on primary grains, implying

communication with an oxygenated atmosphere whereas subsequent deeper burial likely resulted in the addition of late-stage diamagnetic cements that preserve the original detrital quartz signal.

Four MM-1 quartz arenite samples (10.8, 45.3, 47.5, and 74.7 m; Fig. 5e) display elevated κ peaks within quartz and siderite conglomeratic lag deposits. These samples are also associated with higher χ_{lf} values compared to three low χ_{lf} MM-1 sandstone samples (Fig. 11). Hysteresis data indicate that increased κ and χ_{lf} observed in these samples is largely associated with increased paramagnetic contributions similar to the WVGS-4 Fe-carbonate cemented samples (Figs. 13 and 14). Magnetite/titanomagnetite identified in the four high κ MM-1 quartz arenite samples (10.8, 45.3, 47.5, and 74.7 m; Fig. 5e) on the basis of ferrimagnetic loop shape and low to moderate B_{CR} values (e.g. Figs. 6c and d; Fig. 11), likely formed by near-surface oxidation of Fe-carbonate cements following exhumation similar to DDS-12A and DDS-26. The magnetic characteristics of these MM-1 samples also largely agree with those of the WVGS-4 Fe-carbonate cemented sandstones. However, the exact mineralogy and timing of these cements cannot be discerned from the data. Nevertheless, the addition of post-depositional Fe-rich paramagnetic cements can be inferred and are likely the cause of the increased κ and χ_{lf} values observed in these samples.

MM-1 dark mudstone and heterolithic facies are associated with higher κ values than the quartz-arenite facies (Fig, 5e). Elevated values and anomalous peaks are largely attributed to high concentrations of Fe-rich paramagnetic clays and cements as indicated by hysteresis data (Figs. 13 and 14). Low concentrations of magnetite have also been identified in these samples by ferrimagnetic loop characteristics and low B_{CR} values (e.g. Fig. 6c; Fig. 11).

Discussion

Upper Mississippian

Magnetic signals identified in upper Mississippian facies of the Central Appalachian Basin include primary source-area- derived detrital magnetite-titanomagnetite, locally-derived detrital hematite, early diagenetic hematite, and pedogenic enrichment, depletion, amalgamation. Controls on the occurrence of each signal include one or a combination of provenance, climate, landscape position, sediment accumulation or bypass, relative position of base-level, exposure time, water table fluctuations, and redox changes.

Primary detrital magnetite-titanomagnetite identified in the channelized and point-bar sandstones, gray mudstones, and limestones was derived from the Appalachian orogenic province. Its preservation suggests that the sediments were not sufficiently oxidized to form hematite or water-logged to form reduced iron complexes. Detrital hematite identified in the sheet-like sandstone and limestone facies was likely derived from local sources. In the sheet-like sandstone facies, local red siltstone and mudstone intraclasts were incorporated in response to sheet flooding across oxidized floodplain sediments. In these deposits, detrital magnetite/titanomagnetite likely became oxidized as the sediment dewatered on an exposed floodplain.

The magnetic patterns associated with the red and gray vertisol facies largely reflect pedogenic depletion, enrichment, and amalgamation processes attributed to a seasonally wet and dry climate. These magnetic patterns were promoted by the elluviation and illuviation of magnetic species in the surface horizons, as well as vertical mixing in the soil profile by shrink-swell mechanisms. Gray paleosols have been attributed to a high water table resulting in gleying (Retallack et al., 2003) whereas red vertisols indicate highly oxidizing conditions (Retallack, 1988).

Thin intercalated red and gray vertisols (< 2 m) likely reflect short exposure times with a fluctuating water table. During wetter times, thin gray vertisols developed under a seasonal climate in which the wet season was long enough to maintain an elevated water table promoting reduction and mobilization of iron. The ensuing dry season was likely brief and the resulting water-table drop lowered the reduction front enough to allow for some oxidation of magnetite-titanomagnetite and/or Fe-silicates. However, due to the short length of the dry season, complete oxidation to hematite was inhibited. In contrast, the thin red vertisols reflect a shift to a longer dry season in which the water-table remained low allowing magnetite-titanomagnetite and/or Fe-silicates to oxidize to hematite. Thicker red and gray paleosols reflect prolonged periods of exposure and landscape stability, coupled with a fluctuating water table, that resulted in the development stacked paleosol profiles. Similar to the thin gray vertisols, the thick gray vertisols developed during long wet seasons followed by brief dry seasons that inhibited the oxidation of magnetite-titanomagnetite and/or Fe-silicates to hematite. The thick, stacked red vertisols were produced by similar processes to their thinner counterparts, where a long dry season promoted the oxidation of magnetite-titanomagnetite and/or Fe-silicates to hematite, and was followed by a

brief wet season. Miller and Eriksson (1999 and 2000) have inferred that high-amplitude base level changes driven by fourth-order eustatic fluctuations controlled sequence development. These fluctuations were associated with high-frequency climate changes related to global circulation patterns related to waxing and waning of the Gondwanan glaciation. Therefore, changes from wetter to drier times recorded, respectively, in the thick gray and red vertisols may reflect changes in climatic patterns related to glacio-eustacy.

The presence of well-developed paleosols that reflect prolonged exposure and landscape stability are indicative of significant depositional hiatuses and missing intervals of time. Thick paleosols preserved in highstand deposits and reflecting prolonged exposure may represent interfluves correlative with the low-stand surfaces of erosion (Weimer, 1992). Therefore, by recognizing magnetic patterns of enrichment, depletion, and/or amalgamation in diagenetically altered ancient soil profiles lacking obvious pedogenic horizonation, identification of high-frequency climatic-eustatic changes may help in the recognition and interpretion of complex continental successions and assist in sequence stratigraphic analysis.

Lower Pennsylvanian

The primary signals identified in the lower Pennsylvanian quartz arenite facies include early diagenetic magnetite-tiatanomagnetite and siderite, late diagenetic quartz, ankerite, and Fe-dolomite. Signals preserved in the dark mudstone and heterolithic facies are paramagnetically enhanced relative to the quartz arenite facies.

The early and late diagenetic magnetic signals recognized in these facies either preserve or mask the original detrital signals. In the quartz arenite facies, the original depositional signal was diamagnetic as a result of homogeneity within the quartz-rich sediments. Low concentrations of early magnetite-titanomagnetite are insufficient to significantly affect the quartz-dominated magnetic signal. Therefore, the diamagnetic detrital signal is preserved and with progressive burial was amplified by the addition of late stage quartz-cement. Some quartz-rich samples display strong paramagnetic trends that overshadow the diamagnetic effects of the quartz grains. These relationships are attributed to early diagenetic additions of siderite cement and late additions of ankerite, and Fe-dolomite cements. The dark mudstone and heterolithic facies are associated with increases in paramagnetic components largely related to increased Fe-rich clay concentrations.

In fluvial successions like the Raleigh Sandstone, where evidence of pedogenic modification is absent, depositional hiatuses may be identified by evidence of vadose diagenesis. Evidence of vadose diagenesis include: (1) abundant cement, and (2) a loose grain framework, indicating cementation prior to burial compaction (Miall and Arush, 2001). Petrographic and magnetic analyses reveal that siderite cementation occurred early and prior to burial compaction and that siderite cement maintains the open-grain framework in the quartz-rich detrital sediments. Therefore, early siderite cemented zones in the lower Pennsylvanian quartz arenite facies are interpreted to reflect hiatuses in sedimentation.

Identifying surfaces of exposure in multi-story channel-fills has important implications for sequence stratigraphy. Conglomerate lags define multiple episodes of channel incision in the lower Pennsylvanian quartz arenite facies. Blum and Price (1998) have demonstrated that unconformities within Quaternary composite valley-fill sequences represent periods of channel incision and/or sediment bypass along which paleosols developed on abandoned floodplains. In the lower Pennsylvanian quartz arenites, conglomerate lags as well as early siderite cementation zones may reflect periods of prolonged exposure and define unconformities that may be correlative with thick floodplain paleosols indicative of low-stand surfaces of erosion (sequence boundary).

In complex incised valley systems where obvious evidence of erosion and exposure are lacking, magnetic characteristics may be used to identify and characterize stratigraphic surfaces. Recognizing these surfaces within complex, multistory valley-fill successions is important in order to develop a sequence stratigraphic framework. Therefore, applying magnetic techniques to these complex systems may help reveal cryptic surfaces that have regional significance.

Conclusion

Mineral magnetic measurements have helped provide a detailed characterization of magnetic properties within select Carboniferous samples. The results of these analyses suggest that magnetic properties provide useful insights towards identifying the depositional and post-depositional processes and provide a means for recognizing cryptic surfaces that may represent intervals of missing time. Magnetic susceptibility profiles provide a quick and easy means for identifying magnetic patterns. However, there are numerous factors that give rise to the various patterns that cannot be evaluated by susceptibility alone. Therefore, a multi-parameter approach

is essential in order to obtain reliable information pertinent to the argument in question. Our results, combined with a review of previous work, indicate that the magnetic properties of Carboniferous strata can be used to identify depositional, pedogenic, and diagenetic magnetic signals. Furthermore, the results indicate that there are several environmental conditions that give rise to the unique magnetic patterns represented in the study.

1. Mineral magnetic parameters identify primary detrital remanence components in upper Mississippian channelized sandstone, gray mudstone, pointbar sandstone, and limestone facies. Channelized sandstone, gray mudstone, and pointbar sandstone facies contain source-area-derived detrital magnetite/titanomagnetite as the only remanence carrier. Limestone facies contain a mixture of detrital titanomagnetite and hematite largely controlled by sediment influx in response to wet-dry climatic conditions.

2. Magnetic enrichment, depletion, and amalgamation patterns within upper Mississippian red and gray vertisols are indicative of preserved pedogenic signals. These magnetic patterns were produced by the elluviation and illuviation of magnetic species in the surface horizons, as well as vertical mixing in the soil profile by shrink-swell mechanisms. During wetter times, gray vertisols developed under seasonal climates in which the wet season was long enough to maintain an elevated water table to promote reduction and mobilization of iron. The ensuing dry season was likely brief and the resulting water-table drop lowered the reduction front enough to allow for some oxidation of magnetite-titanomagnetite and/or Fe-silicates. Red vertisols likely developed under a long dry season that promoted the oxidation of magnetite-titanomagnetite and/or Fe-silicates to hematite and that was followed by a short wet season. The presence of well-developed paleosols that reflect prolonged exposure and landscape stability are indicative of significant depositional hiatuses and missing intervals of time. These well-developed vertisols reflect significant hiatuses in sedimentation associated with prolonged exposure on interfluve/floodplain surfaces that may correlative with incised valleys.

3. Early and late diagenetic signals are preserved in the lower Pennsylvanian strata. Early diagnenetic signals are preserved in the quartz arenite facies as magnetite and siderite

coatings on detrital grains reflecting early diagenesis under, oxidizing and reducing conditions, respectively. Low concentrations of ferrimagnetic minerals phases are diluted by late burial quartz cements producing dominant diamagnetic hysteresis behavior. The siderite cements record overprinting of the primary detrital signal (diamagnetic) by early paramagnetic cements. Ankerite and Fe-dolomite cements imparted a dominant paramagnetic signal on primary diamagnetic quartz grains during deep burial diagnenesis. These arenites preserve a near-surface ferrimagnetic signal superimposed on a late, deep-burial diagenetic signal. Exhumation likely resulted in near-surface oxidation of these Fe-carbonate cements to form the ferric oxides identified in these samples.

In fluvial successions such as the Raleigh Sandstone, where evidence of pedogenic modification is absent, depositional hiatuses may be identified by evidence of vadose diagenesis preserved in the siderite-cemented, early Pennsylvanian sandstones. The early siderite cements may reflect prolonged subaerial exposure and, together with magnetically distinctive siderite-pebble conglomerate lags, are thought to define unconformities within compound valley fills. Identifying surfaces of exposure in multi-story channel-fills has important implications for developing sequence stratigraphic models for terrigenous siliciclastic sedimentary successions.

References

Begét, J. E., D. B. Stone, and D. B. Hawkins, 1990, Paleoclimatic forcing of magnetic susceptibility variations in Alaskan loess during the late Quaternary: Geology, v. 18, p. 40-43.

Beuthin, J. D., and M. B. Blake, 2002, Scrutiny of a global climate model for Upper Mississippian depositional sequences in the Central Appalachian foreland basin, U.S.A: Journal of Geology, v. 110, p. 739-747.

Blake, M. B., 1997, Revised lithostratigraphy and megafloral biostratigraphy of the New River and Kanawha Formations (Pottsville Group: Lower and Middle Pennsylvanian) in southern West Virginia: M.S. thesis, University of West Virginia, Morgantown, WV, 159 p.

Blum, M. D., and D. M. Price, 1998, Quaternary alluvial plain construction in responce to glacio-eustatic and climatic controls, Texas Gulf Coastal Plain, *in* K. W. Shanley, and P. J. McCabe, eds., Relative Role of Eustacy, Climate, and Tectonism in Continental Rocks, SEPM Special Publication No. 59, p. 31-48.

Burley, S. D., J. D. Kantorowicz, and B. Waugh, 1985, Clastic Diagenesis, *in* P. J. Brenchley, and B. P. J. Williams, eds., Sedimentology: recent developments and applied aspects, v. 18, Geological Society Special Publication, p. 189-226.

Cecil, C. B., 1990, Paleoclimate controls on stratigraphic repetition of chemical and silicicalstic rocks: Geology, v. 18, p. 533-536.

Channell, J. E. T., and C. McCabe, 1994, Comparison of magnetic hysteresis parameters of unremagnetized and remagnetized limestones: Journal of Geophysical Research, v. 99, p. 4613-4623.

Chlachula, J., M. E. Evans, and N. W. Rutter, 1998, A magnetic investigation of a Late Quaternary loess/paleosol record in Siberia: Geophysical Journal International, v. 132, p. 128-132.

Davydov, V., B. R. Wardlaw, and F. M. Gradstein, 2004, The Carboniferous Period, *in* F. M. Gradstein, J. G. Ogg, and A. G. Smith, eds., A Geologic Time Scale 2004: Cambridge, UK, Cambridge University Press, p. 222-248.

Dewey, J.F. 1981. Episodicity, sequence and style at convergent plate boundaries. In The Continental Crust and its Mineral Deposits. Geological Association of Canada, Special Paper 20, 553-572.

Dickinson, W. R., L. S. Beard, G. R. Brakenridge, J. L. Erjavec, R. C. Ferguson, K. F. Inman, R. A. Knepp, F. A. Lindberg, and P. T. Ryberg, 1983, Provenance of North American Phanerozoic sandstones in relation to tectonic setting: Geological Society of America

Bulletin, v. 94, p. 222-235.

Donaldson, A. C., J. J. Renton, and M. W. Presley, 1985, Pennsylvanian deposystems and paleoclimates of the Appalachians: International Journal of Coal Geology, v. 5, p. 167-193.

Driese, S. G., and C. I. Mora, 1993, Physico-chemical environment of pedogenic carbonate formation in Devonian vertic paleosols, central Appalachians, USA: Sedimentology, v. 40, p. 199-216.

Dunlop, D. J., and O. Ozdemir, 1997, Rock Magnetism: Cambridge, UK, Cambridge University Press, 573 p.

Ellwood, B. B., W. Balsam, and B. Burkart, 1986, Anomalous magnetic properties in rocks containing the mineral siderite: paleomagnetic implications: Journal of Geophysical Research, v. 91, p. 12779-12790.

Ellwood, B. B., B. Burkart, K. Rajeshwar, R. L. Darwin, R. A. Neeley, A. B. McCall, G. J. Long, M. L. Buhl, and C. W. Hickcox, 1989, Are the iron carbonate minerals, ankerite and ferroan dolomite, like siderite, important in paleomagnetism?: Journal of Geophysical Research, v. 94, p. 7321-7331.

Ellwood, B. B., T. H. Chrzanowski, F. Hrouda, G. J. Long, and M. L. Buhl, 1988, Siderite formation in anoxic deep-sea sediments: a synergetic bacterially controlled process with important implications in paleomagnetism: Geology, v. 16, p. 980-982.

Ellwood, B. B., R. E. Crick, A. El Hassani, S. Benoist, and R. Young, 2000, Magnetosusceptibility event and cyclostratigraphy method applied to marine rocks: Detrital input versus carbonate productivity: Geology, v. 28, p. 1135-1138.

Englund, K. J., and R. E. Thomas, 1990, Late Paleozoic Depositional Trends in the Central Appalachian Basin: U.S. Geological Survey Bulletin1839-F, p. 19.

Evans, M. E., 2001, Magnetoclimatology of aeolian sediments: Geophysical Journal International, v. 144, p. 495-497.

Evans, M. E., and F. Heller, 1994, Magnetic enhancement and paleoclimate: Study of loess/paleosol couplet across the Loess Plateau of China: Geophysical Journal International, v. 117, p. 257-264.

Evans, M. E., and F. Heller, 2001, Magnetism of loess/ paleosol sequences: recent developments: Earth-Science Reviews, v. 54, p. 129-144.

Florindo, F., R. Zhu, B. Guo, L. Yue, Y. Pan, and F. Speranza, 1999, Magnetic proxy climate results from the Duanjiapo loess section, southernmost extremity of the Chinese loess plateau: Journal of Geophysical Research, v. 104, p. 645-659.

Friedman, G. M., and J. E. Sanders, 1978, Principles of Sedimentolgy, John Wiley and Sons, 792 p.

Geiss, C. E., and S. K. Banerjee, 1997, A multi-parameter magnetic record of the last glacial-interglacial paleoclimate from south-central Illinois, USA: Earth and Planetary Science Letters, v. 152, p. 203-216.

Greb, S. F., D. R. Chesnut, and C. F. Eble, 2004, Temporal changes in coal-vearing depositional sequences (Lower and Middle Pennsylvanian) of the Central Appalachian Basin, U.S.A., *in* J. C. Pashin, and R. A. Gastaldo, eds., Sequence stratigraphy, paleoclimate, and tectonics of coal-bearing strata, AAPG Studies in Geology 51, p. 89-120.

Heller, F., and M. E. Evans, 1995, Loess Magnetism: Reviews of Geophysics, v. 33, p. 211-240.

Heller, F., and T. S. Liu, 1984, Magnetism of Chinese loess deposits: Geophysical Journal of the Royal Astronomical Society, v. 77, p. 125-141.

Houseknecht, D. W., 1980, Comparative anatomy of a Pottsville lithic arenite and quartz arenite of the Pocahontas Basin, southern West Virginia: petrogenetic, depositional, and stratigraphic implications: Journal of Sedimentary Petrology, v. 50, p. 3-20.

Hrouda, F., P. Muller, and J. Hanak, 2003, Repeated progressive heating in susceptibility vs. temperature investigation: a new paleotemperature indicator?: Physics and Chemistry of the Earth, v. 28, p. 653-657.

Klein, G. d., and D. A. Willard, 1989, The origin of the Pennsylvanian coal-bearing cyclothems of North America: Geology, v. 17, p. 152-155.

Kontny, A., H. De Wall, T. G. Sharp, and M. Posfai, 2000, Mineralogy and magnetic behavior of pyrrhotite from a 260^{o}C section at the KTB drilling site, Germany: American Mineralogist, v. 85, p. 1416-1427.

Korus, J. T., 2002, The Lower Pennsylvanian New River Formation: A Nonmarine Record of Glacioeustasy in a Forland Basin: M.S. thesis, Virginia Polytechnic Institute and State University, Blacksburg, VA, 54 p.

Kraus, M. J., and T. M. Bown, 1988, Pedofacies Analysis; a new approach to reconstructing ancient fluvial sequences, *in* J. Reinhardt, and W. R. Sigleo, eds., Paleosols and Weathering Through Geologic Time: Principles and Applications, Geological Society of America Special Paper 216, p. 143-152.

Kukla, G., F. Heller, X. M. Liu, T. C. Xu, T. S. Liu, and Z. S. An, 1988, Pleistocene climates in China dated by magnetic susceptibility: Geology, v. 16, p. 811-814.

Kvale, E. P., A. W. Archer, and H. R. Johnson, 1989, Tidal deposits associated with low-sulfur

coals, Brazil Fm. (Lower Pennsylvanian), Indiana: Journal of Sedimentary Petrology, v. 60, p. 563-574.

Kvale, E. P., J. Cutright, D. Bilodea, A. W. Archer, H. R. Johnson, and B. Pickett, 1995, Analysis of modern tides and implications for ancient tidalites: Continental Shelf Research, v. 15, p. 1921-1943.

Liu, J., R. Zhu, A. Roberts, S. Li, and J.-H. Chang, 2004, High-resolution analysis of early diagenetic effects on magnetic minerals in post-middle-Holocene continental shelf sediments from the Korea Strait: Journal of Geophysical Research, v. 109, p. B03103.

Liu, Q., C. Deng, Y. Yu, J. Torrent, M. Jackson, S. Banerjee, and R. Zhu, 2005, Temperature dependence of magnetic susceptibility in an argon environment: implications for pedogenesis of Chinese loess/paleosols: Geophysical Journal International, v. 161, p. 102-112.

Liu, X. M., J. Shaw, T. S. Liu, F. Heller, and Y. Baoyin, 1992, Magnetic mineralogy of Chinese loess and its significance: Geophysical Journal International, v. 108, p. 301-308.

Mack, G. H., W. C. James, and H. C. Monger, 1993, Classification of paleosols: Geological Society of America Bulletin, v. 105, p. 129-136.

Maher, B. A., 1998, Magnetic properties of modern soils and Quaternary loessic paleosols: paleoclimatic implications: Paleogeography, Paleoclimatology, Paleoecology, v. 137, p. 25-54.

Maher, B. A., and R. Thompson, 1995, Paleoainfall reconstructions from pedogenic magnetic susceptibility variations in the Chinese loess and paleosols: Quaternary Research, v. 44, p. 383-391.

McDowell, R. J., 1986, An interpretation of the Grafton sandstone and its implications for Pennsylvanian paleohydraulics, climate, provenance, and tectonics: Compass of Sigma Gamma Epsilon, v. 63, p. 161-190.

Miall, A. D., and M. Arush, 2001, Cryptic sequence boundaries in braided fluvial successions: Sedimentology, v. 48, p. 971-985.

Miller, D. J., 1998, Depositional Environments and Sequence Stratigraphy of Upper Mississippian Strata in the Central Appalachian Basin: Ph.D. thesis, Virginia Polytechnic Institute and State University, Blacksburg, VA, 87 p.

Miller, D. J., and K. A. Eriksson, 1999, Linked sequence development and global climate change: The Upper Mississippian record in the Appalachian basin: Geology, v. 27, p. 35-38.

Miller, D. J., and K. A. Eriksson, 2000, Sequence stratigraphy of Upper Mississippian strata in

the Central Appalachians: A record of glacioeustasy and tectonoeustasy in a foreland basin setting: AAPG Bulletin, v. 84, p. 210-233.

Mozely, P. S., 1989, Relation between depositional environment and the elemental composition of early diagenetic siderite: Geology, v. 17, p. 704-706.

Ozdemir, O., and D. J. Dunlop, 2000, Intermediate magnetite formation during dehydration of goethite: Earth and Planetary Science Letters, v. 177, p. 59-67.

Pan, Y., R. Zhu, S. K. Banerjee, J. Gill, and Q. Williams, 2000, Rock magnetic properties related to thermal treatment of siderite: Behavior and interpretation: Journal of Geophysical Research, v. 105, p. 783-794.

Peters, C., and M. J. Dekkers, 2003, Selected room temperature magnetic parameters as a function of mineralogy, concentration and grain size: Physics and Chemistry of the Earth, v. 28, p. 659-667.

Platt, N. H., and V. P. Wright, 1991, Lacustrine carbonates, *in* P. Anason, L. Cabrera, and K. Kelts, eds., Lacustrine Facies Analysis, Special Publication 13, International Association of Sedimentologists, Blackwell Scientific Publications, Oxford, p. 57-74.

Postma, D., 1982, Pyrite and siderite formation on brackish and freshwater swamp sediments: American Journal of Science, v. 282, p. 1151-1183.

Price, G. D., P. J. Valdes, and B. W. Sellwood, 1997, Prediction of modern bauxite occurrence: implications for climate reconstruction: Paleogeography, Paleoclimatology, Paleoecology, v. 131, p. 1-13.

Quinlan, G. M., and C. Beaumont, 1984, Appalachian thrusting, lithospheric flexure, and Paleozoic stratigraphy of eastern North America: Canadian Journal of Earth Sciences, v. 21, p. 973-976.

Rankey, E. C., and M. R. Farr, 1997, Preserved pedogenic mineral magnetic signature, pedogenesis, and paleoclimate change: Pennsylvanian Roca Shale (Virgilian, Asselian), central Kansas, USA: Sedimentary Geology, v. 114, p. 11-32.

Reed, J. S., K. A. Eriksson, and M. Kowalewski, 2005, Climate, depositional and burial controls on diagenesis of Appalachian Carboniferous sandstones: qualitative and quantitative methods: Sedimentary Geology, v. 176, p. 225-246.

Reineck, H.-E., and F. Wunderlich, 1968, Classification and origin of flaser and lenticular bedding: Sedimentology, v. 11, p. 99-104.

Retallack, G. J., 1988, Field Recognition of Paleosols, *in* J. Reinhardt, and W. R. Sigleo, eds., Paleosols ans Weathering Through Geologic Time, Geological Society of America Special Paper 216, p. 1-20.

Retallack, G. J., N. D. Sheldon, M. Cogoini, and R. D. Elmore, 2003, Magnetic susceptibility of early Paleozoic and Precambrian paleosols: Paleogeography, Paleoclimatology, Paleoecology, v. 198, p. 373-380.

Riley, N., and N. Turner, 1995, The correlation of mid-Westphalian marine bands between the central Appalachian Basin (USA) and the United Kingdom: XIII International Congress of Carboniferous-Permian, Krakhow, Poland, p. 122.

Rochette, P., G. Fillio, J. L. Mattei, and M. J. Dekkers, 1990, Magnetic transitions at 30-40 Kelvin in pyrrhotite: insight into a widespread occurrence of this mineral in rocks: Earth and Planetary Science Letters, v. 98, p. 319-328.

Soregan, G. S., R. D. Elmore, B. Klatz, M. Cogoini, and S. Banerjee, 1997, Pedogenically enhanced magnetic susceptibility variations in Paleozoic loessite: Geology, v. 25, p. 1003-1006.

Soreghan, G. S., R. D. Elmore, and M. T. Lewchuk, 2002, Sedimentologic-magnetic record of western Pangean climate in Paleozoic loessite (lower Cutler beds, Utah): GSA Bulletin, v. 114, p. 1019-1035.

Swezey, C. S., 2002, Regional stratigraphy and petroleum systems of the Appalachian Basin, North America: U.S. Geological Survey Geologic Investigation Series Map I-2768.

Theveniaut, H., and P. Freyssinet, 1999, Paleomagnetism applied to lateritic profiles to assess saprolite and duricrust formation processes: the example of Mont Baduel profile (Frnch Guiana): Paleogeography, Paleoclimatology, Paleoecology, v. 148, p. 209-231.

Torii, M., K. Fukuma, C.-S. Horng, and T.-Q. Lee, 1996, Magnetic discrimination of pyrrhoite- and greigite-bearing sediment samples: Geophysical Research Letters, v. 23, p. 1813-1816.

Tsatskin, A., F. Heller, E. A. Hailwood, T. S. Gendler, J. Hus, P. Montgomery, M. Sartori, and E. I. Virina, 1998, Pedosedimentary division, rock magnetism and chronology of the loess/paleosol sequence at Roxolany (Ukraine): Paleogeography, Paleoclimatology, Paleoecology, v. 143, p. 111-133.

Turner, B. R., and K. A. Eriksson, 1999, Meander bend reconstruction from an Upper Mississippian point bar at Possum Hollow, West Virginia, USA: Special Publication of the International Association of Sedimentologits, v. 28, p. 363-379.

Verosub, K. L., P. Fine, M. J. Singer, and J. TenPas, 1993, Pedogenesis and paleoclimate: Interpretation of the magnetic susceptibility record of Chinese loess-paleosol sequences: Geology, v. 21, p. 1011-1014.

Verosub, K. L., and A. Roberts, 1995, Environmental magnetism: Past, present, and future:

Journal of Geophysical Research, v. 100, p. 2175-2192.

Virina, E. I., S. S. Faustov, and F. Heller, 2000, Magnetism of loess-paleosol formations in relation to soil-forming and sedimentary processes: Physics and Chemistry of the Earth, v. 25, p. 475-478.

Weimer, R. J., 1992, Developments in sequence stratigraphy: forland and cratonic basins: AAPG Bulletin, v. 76, p. 965-982.

Zhu, R., C. Shi, V. Suchy, A. Zeman, B. Guo, and Y. Pan, 2001, Magnetic properties and paleoclimatic implications of loess-paleosol sequences of Czech Republic: Science in China (Series D), v. 44, p. 385-394.

Appendix Contents

Appendix A – Magnetic Theory and Background……62
Magnetic Susceptibility…...……62
Hysteresis Parameters.....63
Magnetic Mineral Types.....64
Magnetic Grain Size……67
Interpretting Hysteresis Loops and Parameters……...68
Thermal Magnetic Analyses……..……71
Figures……..73
Figure Captions…….……...75
References……....76
Appendix B – WVGS-4 Magnetic Characterization (Upper and Lower Raleigh Sandstones)....78
Figures……..86
Figure Captions…….……...98
References…….……...99
Appendix C – MM-1 Magnetic Characterization (Lower Pennsylvanian New River Fm.)…...100
Figures……107
Figure Captions……..116
References……..116
Appendix D – SSWV-1 Magnetic Characterization (Lower Hinton Fm. Stony Gap Mem.)….117
Figures……126
Figure Captions……..137
References……..137
Appendix E – PWV-1 Magnetic Characterization (Upper Hinton Fm.)……...….138
Figures……144
Figure Captions……..156
References……..156
Appendix F – PHS-1 Magnetic Characterization (Upper Mississippian Hinton Fm.)……..….157
Figures……162
Figure Captions……..170
References……..170